plants, algae, yeast, slime molds, free-living amoebae, eubacteria and nematodes [13–16]. Moreover, recent bioinformatic searches have broadened the taxonomic distribution of AOX to some members of the animal kingdom [17]. The primary role of AOX in non-thermogenic plants is to regulate cellular redox balance and to protect against reactive oxygen species particularly when the cytochrome pathway is inhibited [18–20]. In addition to this role, many other physiological roles have been described for AOXs in other organisms and these have been discussed in detail elsewhere [13,21]. The ubiquitous occurrence of AOX may suggest that the metabolic flexibility that the alternative pathway confers upon an organism allows it to respond to a wide range of developmental and environmental conditions [22].

Despite universal conservation of the gene and diversified physiology, the molecular features of AOX have not yet been well characterized. Although no high-resolution AOX structure has been determined to date, current structural models predict that it is an integral interfacial membrane protein that interacts with a single leaflet of the lipid bilayer, and contains a non-haem diiron carboxylate active site [23,24]. This model is supported by extensive site-directed mutagenesis studies [18,25–29] and furthermore both EPR and FTIR spectroscopies have confirmed the presence of a binuclear iron center in both the plant and trypanosomal enzymes [30–32].

Further detailed structural and biochemical analyses of AOXs, however, requires further development of purification protocols to produce sufficiently purified and highly active protein to enable crystallization trials and kinetic analyses to proceed. In this paper, we report on the further refinement of our previous protocol through over-expressing rTAO in an *E. coli ΔhemA* mutant (FN102) strain, which lacks quinol oxidase activity of cytochrome *bo* and *bd* complexes [33–35]. Purified rTAO protein is highly active and exhibits an exceptional stability upon storage. The analysis of the prosthetic groups by inductively coupled plasma-mass spectrometer (ICP-MS) and electron paramagnetic resonance (EPR) reveals the presence of two ferric ions stoichiometrically bound per rTAO monomer. To our knowledge this is the first direct confirmation of two ferric irons per AOX. Furthermore we show that purified rTAO is potently inhibited by ascofuranone with mixed function kinetics.

2. Materials and methods

2.1. Preparation of membrane sample

The strain FN102/pTbAO carrying cDNA for *T. b. brucei* TAO [36] was pre-cultured at 37 °C in 100 ml of LB medium containing 10 mg ampicillin, 5 mg kanamycin, and 5 mg 5-aminolevulinic acid for 4–6 h. The pre-cultured cells were aerobically grown at 30 °C in 10 l of S-medium containing 100 g tryptone peptone, 50 g yeast extract, 50 g casamino acid, 104 g K_2HPO_4, 30 g KH_2PO_4, 7.5 g trisodium-citrate·$2H_2O$, 25 g $(NH_4)_2SO_4$, 0.5 g $MgSO_4 \cdot 7H_2O$, 0.25 g $FeSO_4 \cdot 7H_2O$, 0.25 g $FeCl_3$, 0.2%(w/v) glucose, and 1 g carbenicillin. The culture was initiated at O.D_{600} = 0.01 and expression of rTAO was induced by the addition of isopropyl β-D-1-thiogalactoside (IPTG) (25 μM) at O.D_{600} = 0.1. Cells were harvested 8–10 h following induction and were resuspended in 50 mM Tris–HCl (pH 7.5) containing 20%(w/w) sucrose, 0.1 mM phenylmethane sulfonyl fluoride (PMSF) and protease inhibitor cocktail (Sigma) and broken by a French Pressure Cell (Ohtake, Tokyo). Unbroken cells were removed by centrifugation at 8000 *g* for 10 min (Hitachi 21G). Inner membranes of FN102/pTbAO were fractionated in high density sucrose after ultracentrifugation at 200,000 *g* for 1 h at 4 °C (Hitachi 85H) (35 ml of supernatant was overlaid over 35 ml of 50 mM Tris–HCl pH 7.5 containing 40%(w/w) sucrose per ultracentrifuge tube). Buoyant inner rich membranes upon 40%(w/w) sucrose layer were fractionated and the inner membrane pellet was separated by further ultracentrifugation at 200,000 *g* for 1 h (HITACHI 85H). The membrane pellet was resuspended in 50 mM Tris–HCl (pH 7.5) containing 20%(w/w) sucrose.

2.2. Solubilization

Membranes were treated with solubilization buffer (6 mg/ml protein in 50 mM Tris–HCl, 1.4%(w/v) *n*-octyl-β-D-glucopyranoside (OG), 200 mM $MgSO_4$, 20%(v/v) glycerol, pH 7.3) at 4 °C and immediately ultracentrifuged at 200,000 *g* for 1 h at 4 °C. The quinol oxidase activities of the samples before centrifugation, as well as that of supernatant and pellet were determined.

2.3. Purification of rTAO

Hybrid batch/column procedure described in the manufacturer's instruction was used as stated below. Ten milliliter of the resin (BD Bioscience, TALON Metal Affinity Resin) was equilibrated in a batch format by 100 ml of equilibration buffer (20 mM Tris–HCl, 1.4%(w/v) OG, 100 mM $MgSO_4$, 20%(v/v) glycerol, pH 7.3). Twenty milliliter of OG extract was mixed with the resin for 20 min at 4 °C. The resin was washed twice with 100 ml of wash buffer (20 mM Tris–HCl, 20 mM imidazole, 0.042%(w/v) *n*-dodecyl-β-D-maltopyranoside (DM), 50 mM $MgSO_4$, 20%(v/v) glycerol pH 7.3) and the resin bound rTAO was transferred to a column for additional washing with 20 ml of second wash buffer (20 mM Tris–HCl, 165 mM imidazole, 0.042%(w/v) DM, 50 mM $MgSO_4$, 20%(v/v) glycerol pH 7.3; flow rate 1 ml/min) and protein elution. Finally, rTAO was eluted with elution buffer (20 mM Tris–HCl, 200 mM imidazole, 0.042%(w/v) DM, 50 mM $MgSO_4$, 60 mM NaCl, 20%(v/v) glycerol pH 7.3; flow rate 1 ml/min). Fractions (4 ml each) were collected.

2.4. Quantitative analysis of metals and EPR spectroscopy

Three independent preparations of rTAO were analyzed (details in Section 3). Each sample solution containing 0.1 g of rTAO was added to 1 ml of nitric acid and 7 ml of water. Organic compounds were hydrolyzed by microwave-assisted protein digestion system (Ethos Pro, Milestone General). Fe, Mn, Cu, Zn and Co in each sample were quantified by inductively coupled plasma-mass spectrometer (ICP-MS, ELAN DRC PerkinElmer Japan). Analysis was performed by the Sumika Chemical Analysis Center (Osaka, Japan). Protein concentration was determined by the Lowry method.

EPR spectra were recorded on a JEOL X-band JES-FA300 spectrometer equipped with an ES-CT470 Heli-Tran cryostat system and a Scientific Instruments digital temperature indicator/controller model 9700a. For EPR analysis of rTAO, 13 mg/ml purified rTAO was frozen in EPR tubes in liquid nitrogen. The purified rTAO was reduced by 2 mM dithionite and 1 mM phenazine methosulfate prior to freezing.

2.5. Ubiquinol oxidase assay

Ubiquinol oxidase activity was measured by recording the absorbance change of ubiquinol-1 at 278 nm (Shimadzu spectrophotometer UV-3000). Reactions were started by the addition of ubiquinol-1 (final concentration 150 μM, $\varepsilon_{278} = 15{,}000\ M^{-1}\ cm^{-1}$) after 2 min preincubation at 25 °C in the presence of rTAO and 50 mM Tris–HCl (pH 7.4). For the enzyme kinetics of purified rTAO, the reaction was initiated by the addition of ubiquinol-1 after 2 min preincubation at 25 °C in the presence of rTAO and 50 mM Tris–HCl (pH 7.4) containing 0.05%(w/v) octaethylene glycol-monododecylether detergent (C10E8).

2.6. Chemicals

All chemicals were biochemistry grade. Ubiquinone-1 and protease inhibitor cocktail were purchased from Sigma-Aldrich. The other detergents were purchased from Dojin Chemicals (Tokyo, Japan).

3. Results

3.1. Purification of fully active TAO

Although we previously established a protocol for the overproduction of rTAO in *E. coli* FN102 (*ΔhemA*) lacking cytochrome *bo* and *bd* complexes of the bacteria, the yield of the active enzyme was too low to analyze its prosthetic group [36]. Such a preparation also hampered the determination of kinetic parameters of rTAO such as its molecular activity. Therefore, conditions for the expression of rTAO and purification protocols were optimized to obtain large quantities of active and stable rTAO to enable such determinations. Three factors were critical to obtain large amounts of active rTAO, namely, growth time of the culture prior to addition of IPTG, absolute concentration of IPTG, and the use of purified inner membranes as the starting material.

After extensive screening of detergents and additives to establish the procedure for efficient extraction of active rTAO from the inner membranes, we found that *n*-octyl-β-D-glucopyranoside (OG) specifically solubilized rTAO as shown in Table 1 (specific activity increased from 23.3 to 63.2 μmol/min/mg after solubilization). Approximately 60% of the membrane quinol oxidase activity was recovered with 1.4%(w/v) OG in the extract (Sup. Fig. 1). Thus, recovery of the activity was significantly higher than that of previously reported digitonin extraction (17%) [36]. Following solubilization, it was possible to maintain enzymatic activity for at least 1 month at 20 °C.

Since rTAO was fused with N-terminal histidine tag, solubilized rTAO was purified by cobalt affinity chromatography. Although the enzyme solubilized by OG was bound to the cobalt affinity resin in the presence of OG, it was not possible to elute bound rTAO from the resin with buffer containing OG. Interestingly, however, we found that 100% of the rTAO activity could be recovered from the column when OG in the washing and elution buffers was exchanged with *n*-dodecyl-β-D-maltopyranoside (DM). In the final step, purified rTAO was obtained by a two-step elution with 165 mM and 200 mM imidazole, which resulted in a very efficient purification of active rTAO in the presence of DM. A typical elution profile of quinol oxidase activity with increasing imidazole concentration is shown in Sup. Fig. 1B. Purified rTAO, with a molecular mass of 34 kDa, was estimated to be 95% pure by SDS-PAGE (Fig. 1A, lane 5). In addition to the 34 kDa band, it is apparent that other bands are also present including two with a smaller size than rTAO and one band with an approximate molecular mass of 74 kDa. Since all of these bands were recognized in Western blot using a monoclonal antibody against TAO (Fig. 1B), the smaller protein bands possibly represent proteolytic breakdown products whilst the 74 kDa band most likely represents the dimeric form of rTAO. The specific activity of purified rTAO was more than 200 μmol/min/mg protein when 150 μM of ubiquinol-1 was used as a substrate, which had a five-fold higher activity than that of the previously purified rTAO (approximately 40 μmol/min/mg) [36]. Quinol oxidase activity of purified rTAO was insensitive to 5 mM KCN but was completely inhibited by 10 nM ascofuranone. A greater than 35-fold increase in purification was achieved using the techniques described above, and 13.2% of the total activity was recovered from the lysate of FN102/pTAO cells as summarized in Table 1. Such procedures resulted in approximately 10 mg of highly purified rTAO from a 10 l culture.

Table 1
Purification of rTAO.

Fractions	Total activity (μmol/min)	Protein (mg)	Specific activity (μmol/min/mg)	Recovery (%)
E. coli lysate	14100	2410	5.85	100
Inner membrane	3500	150	23.3	24.8
OG extract	2400	37.9	63.2	17.0
Co-column	1860	8.95	207	13.2

The activities listed here were measured using 150 μM of ubiquinol-1. Fractions (eluate numbers 6–13 in Supplemental Fig. 1B) were collected as purified rTAO after co-column.

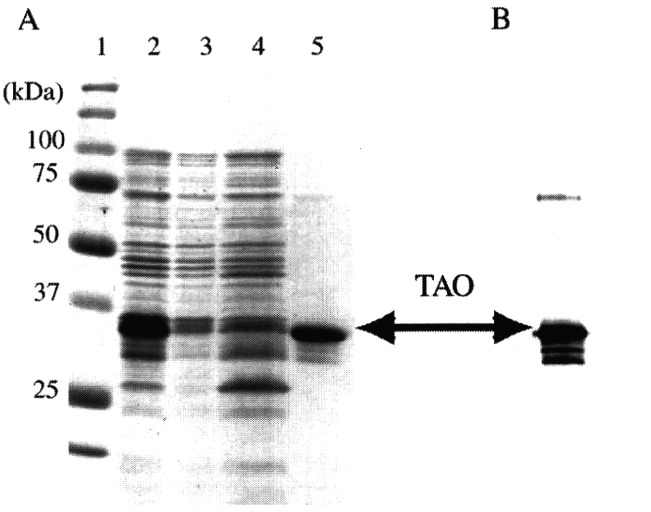

Fig. 1. SDS-PAGE and Western blotting of rTAO in purification steps. A: CBB-staining 12.5% SDS-PAGE of each fraction from the cobalt column chromatography. Lane 1, marker; lanes 2 and 3, each 5 ml of OG extract and flow through fraction; lane 4, 500 ml of wash fraction; and lane 5, 60 ml of eluted fraction collected from fractions 6–12. Loading samples on lanes 2 to 5 were precipitated with acetone. B: Western blot of purified rTAO. The same sample to lane 5 in panel B was electrophoresed on 12.5% polyacrylamide gel. Monoclonal antibodies were used against highly purified rTAO obtained by a nickel column in the presence of guanidine. Epitope recognized by this antibody is the C-terminal domain of the enzyme. The arrow indicates rTAO with an apparent molecular mass of 34 kDa.

3.2. Iron content in purified TAO

Since a highly active and stable purified rTAO could be obtained by the protocol described above, the metal content of purified rTAO was measured by ICP-MS. On the basis that TAO has a diiron center as previously proposed [23,24], then two equivalents of iron should be detected per monomer of rTAO. To this end we analyzed the iron content of purified native rTAO, inactive rTAO, denatured rTAO, and iron within the buffer eluted from the cobalt-column. Purified native rTAOs derived from three independent *E. coli* cultures were precipitated by PEG 3350 and resuspended in the elution buffer at three different concentrations as shown in Sup. Table 1. To prepare inactive rTAO, precipitated rTAO was resuspended in 50 mM Tris–HCl pH 7.4, which resulted in complete loss of enzyme activity. Denatured rTAO was prepared by resuspending the precipitant in elution buffer containing 6 M guanidine–HCl and 0.3 M EDTA. Metal contents in these preparations were 9000 ng/ml, 2900 ng/ml and 1800 ng/ml of Fe respectively for the native rTAO (3.71, 1.19 and 0.80 mg/ml), 230 ng/ml, 100 ng/ml and 28 ng/ml of Fe for inactive rTAO, denatured rTAO and the elution buffer, respectively (Sup. Table 1). From these results, the stoichiometry of bound iron per rTAO monomer can be deduced as indicated below, based on the following parameters namely, a molecular mass of rTAO of 39,391 Da (including the 6× histidine tag), purity of 95% based on SDS-PAGE gels, and the atomic weight of Fe being 55.85. Thus the ratio of iron atoms per rTAO is 1.76 for native rTAO and 0.2 and 0.08 in inactive rTAO and denatured rTAO, respectively (Table 2). This data indicates that one monomer of TAO possesses two atoms of iron which are released during inactivation or denaturation of the enzyme. To our knowledge, this is the first direct measurement of iron in purified AOX and the stoichiometry is consistent with the active site of AOX being a diiron carboxylate-center.

Other metals including Mn, Cu and Zn were also analyzed (Sup. Table 1). In all cases, these metals were below their detection limit (10 ng/ml sample solution) or background level. Although cobalt was

Table 2
Ratio of metals to purified rTAO.

	Fe/rTAO	Zn/rTAO	Mn/rTAO	Cu/rTAO
	Mean ± S.D.			
Native rTAO	1.76 ± 0.077	0.03 ± 0.013	N.D.[a]	N.D.
Inactive rTAO	0.22[b]	N.D.	N.D.	N.D.
Denatured rTAO	0.08[b]	N.D.	N.D.	N.D.

Stoichiometric ratio of metals to one molecular TAO was calculated using data in Supplemental Table 1.
[a] N.D. represents Not Detected (below 0.01).
[b] The value is an average of two independent experiments.

detected in purified rTAO, its concentration was comparable to that of cobalt in the elution buffer derived from the resin (data not shown). Similarly although 130 ng/ml, 66 ng/ml and 61 ng/ml of Zn were detected in native rTAO, these amounts of Zn were not commensurate with that of the enzyme stoichiometry. The detected Zn might be derived from the Zn-substituted form of rTAO, which was suggested to be possible from structural analysis [37]. In addition, at least 90% of the purified rTAO retained its prosthetic group in its active form.

In addition to measuring the stoichiometry of iron in purified rTAO, EPR analysis of purified rTAO was also performed in order to confirm that purified rTAO was indeed a diiron carboxylate protein and whether the detected iron originated from a diiron binding center. As shown in Fig. 2, a low field EPR signal at approximately $g = 15$ in the perpendicular EPR mode was observed with the reduced form of rTAO when the enzyme was reduced by 2 mM of dithionite and 1 mM of phenazine methosulfate (PMS), although the intensity of the signal was low. Importantly the signal disappeared in the oxidized form of rTAO. This low field EPR signal is characteristic for diiron proteins and is ascribed to an exchange-coupled high spin ferrous iron [38]. Although this signal is not normally observed in the perpendicular mode, it can be detected under certain conditions as outlined in this report [39]. The effective g-value of 15 observed in the perpendicular mode is slightly lower than the value of 16 previously observed by us [31] but this is probably due to the fact that parallel-mode EPR spectroscopy is a much more sensitive probe than the perpendicular mode. Nevertheless the finding of a low field signal when the purified enzyme is reduced is further confirmation that the purified rTAO we report here is indeed a diiron carboxylate protein. It should be noted however that we were unable to observe the $g = 15$ signal when the enzyme was reduced by more physiological reductants such as ubiquinol-1 the reasons for which are, at present, unclear.

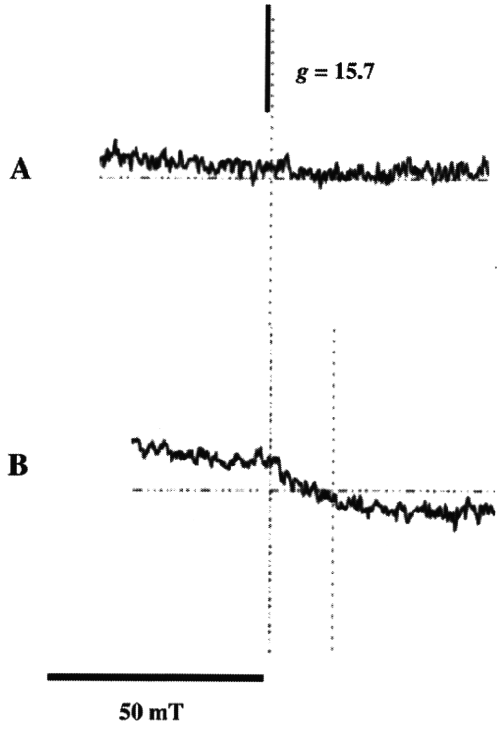

Fig. 2. EPR spectra of rTAO. A: Oxidized form of rTAO (360 μM). B: Reduced form of rTAO (360 μM), which was treated by 2 mM of dithionite and 1 mM phenazine methosulfate for 30 min on ice. Instrument parameters: microwave frequency, 9.02 GHz; microwave power, 1 mW; modulation frequency, 100 kHz; modulation amplitude, 0.6 mT; and temperature of 5 K.

3.3. Kinetic properties of purified TAO

Kinetic analysis of purified rTAO (or AOX) using ubiquinone analogs has previously proved difficult because: 1) the enzyme, following solubilization, was extremely unstable, 2) the natural substrate of trypanosome AOX is ubiquinol-9 [4], which is too hydrophobic to use as the substrate in the assay and 3) the enzymatic activity was not saturated at the maximum concentration of ubiquinol-1 (approximately 300 μM). Since we have purified rTAO in a fully active form and confirmed the stoichiometric presence of the diiron center, the purified rTAO was well-suited to a kinetic analysis.

As noted in our earlier study [36] and in AOXs from other organisms [40] non Michaelis–Menten kinetics is observed when ubiquinol-1 is used as a substrate. Hoefnagel et al. [40], however, observed that the addition of a specific detergent (0.025% EDT-20) during the assay increased the activity by 3- to 4-fold close to saturation. Although the addition of 0.025%(w/v) of EDT-20 equally enhanced the activity of purified rTAO by approximately 2-fold, it did have a deleterious effect upon the long term stability of the enzyme (Sup. Fig. 2).

In an attempt to overcome this problem, various detergents were therefore screened to determine if they could enhance activity without affecting enzyme stability. When the effect of the detergents on enzyme activity was evaluated by monitoring the activity of rTAO in the presence of detergent (Sup. Fig. 3), most activity was retained in the presence of 0.05%(w/v) of C10E8 (Sup. Fig. 4A). Light scattering at 400 nm confirmed that at least 600 μM of ubiquinol-1 was soluble in the assay system (Sup. Fig. 4B). The kinetics of ubiquinol-1 oxidation by purified rTAO in the presence of 0.05%(w/v) of C10E8 showed typical Michaelis–Menten kinetics (Fig. 3, K_m of 338 ± 23.2 μM and V_{max} of 601 ± 27.0 μmol/min/mg). In contrast, activity was linearly dependent upon substrate concentration in the absence of detergent indicating unsaturation in agreement with previous studies [36,40] (Fig. 4). Enzymatic analysis was performed with a wide range of

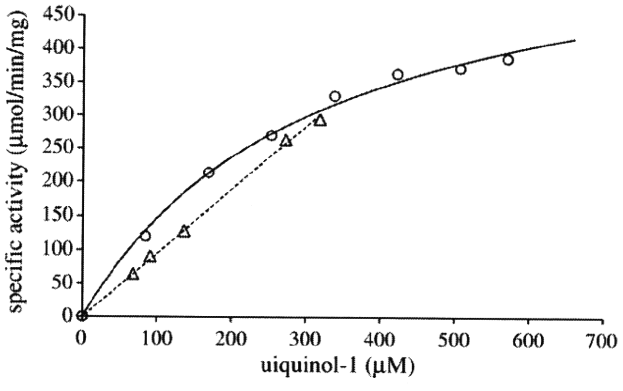

Fig. 3. Kinetics of ubiquinol-1 oxidation by purified rTAO. S–V plot of ubiquinol oxidase activity is shown using 75 ng of purified rTAO in 50 mM Tris–HCl (pH 7.4) and ubiquinol-1 (80–580 μM) with (○) and without (△) 0.05%(w/v) C10E8 at 25 °C. The solid line indicates the fitted Michaelis–Menten kinetics with the detergent (K_m of 338 ± 23.2 μM and V_{max} of 601 ± 27.0 μmol/min/mg), whereas the dashed line indicates the linear relationship between the substrate concentration and the activity without the detergent.

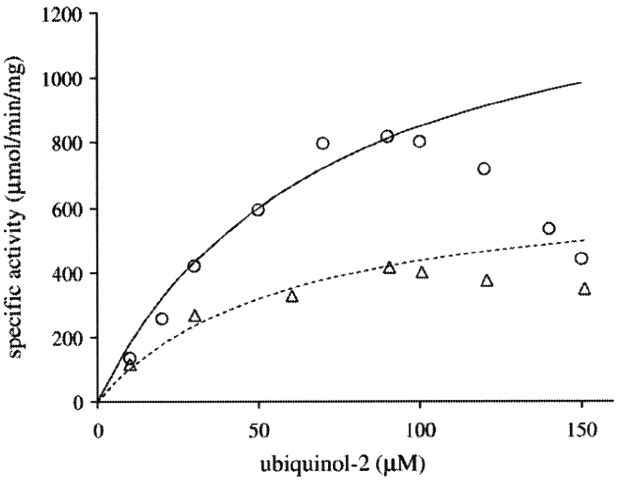

Fig. 4. Kinetics of ubiquinol-2 oxidation by purified rTAO. S–V plot of ubiquinol oxidase activity is shown using 75 ng of purified rTAO in 50 mM Tris–HCl (pH 7.4) and ubiquinol-2 (10–150 μM) with (△) 0.05%(w/v) C10E8 and with (○) 0.025%(w/v) EDT-20 at 25 °C. The solid line indicates the fitted Michaelis–Menten kinetics in the concentration range below 90 μM of ubiquinol-2 with 0.025%(w/v) EDT-20, whereas the dashed line does with 0.05%(w/v) C10E8 (K_m of 71 ± 1.2 μM and V_{max} of 1,460 ± 53.2 μmol/min/mg with 0.025%(w/v) EDT-20, whereas K_m of 57 ± 8.5 μM and V_{max} of 691 ± 28.0 μmol/min/mg with 0.05%(w/v) C10E8).

substrate concentrations (80–570 μM), which corresponded to 0.4 K_m–1.7 K_m.

To investigate whether the length of the side chain of the substrate affected the kinetic properties of rTAO, a kinetic analysis using ubiquinol-2 in the presence of EDT-20 and C10E8 (Fig. 4) was performed. Fig. 4 indicates that during the oxidation of ubiquinol-2, enzyme activity decreased above 100 μM substrate even in buffers containing either detergent. Although kinetic parameters using ubiquinol-2 could not be obtained due to substrate inhibition, S–V plots in the concentration range below 90 μM of ubiquinol-2 could be used to qualitatively analyze the effects of side chain on enzyme activity. Calculated values from such plots revealed that in the presence of 0.025%(w/v) EDT-20 the K_m (ubiquinol-2) was 71 ± 1.2 μM and V_{max} = 1460 ± 53.2 μmol/min/mg whereas with, 0.05%(w/v) C10E8 the K_m was 57 ± 8.5 μM and V_{max} = 691 ± 28.0 μmol/min/mg.

Ascofuranone is a highly specific and potent inhibitor of TAO [7] and it was therefore of importance to determine its inhibitory effect on ubiquinol-1 oxidation by purified rTAO in the presence of 0.05%(w/v) of C10E8 (Sup. Fig. 5A). From the data presented in Sup. Fig. 5A the apparent kinetic parameters of ubiquinol-1 oxidation in the presence of 0.5 nM and 2 nM of ascofuranone were estimated to be respectively $K_m^{0.5\,nM}$ = 368 ± 6.4 μM; $V_{max}^{0.5\,nM}$ = 490 ± 22.4 μmol/min/mg and $K_m^{2\,nM}$ = 492 ± 7.2 μM; and $V_{max}^{2\,nM}$ = 309 ± 60.5 μmol/min/mg. The increased K_m and decreased V_{max} values (Sup. Fig. 5B) indicate that ascofuranone inhibits purified rTAO in a mixed-type non-competitive manner with respect to ubiquinol-1.

4. Discussion

The overall goal of the present study was to obtain a highly pure and stable rTAO protein with maximum specific activity which could be used to investigate the kinetic properties of the enzyme. The quality of the purified rTAO obtained in this study has resulted in three important aspects with respect to the structure of AOX namely, the first direct evidence of stoichiometrically bound iron within the diiron center of rTAO, secondly reliable measurements of kinetic parameters and thirdly that a sample of sufficient purity and yield could be produced that has resulted in the formation of crystals [41].

4.1. Overexpression and purification of rTAO

The difficulties in isolating stable AOXs in an active form have hampered the biochemical and structural analyses of the enzyme including identification of its prosthetic groups, tertiary structural analysis and the definition of enzyme kinetic parameters. The present study reports on the overexpression and purification of active rTAO, which has enabled us to study biochemical and protein chemistry properties of this enzyme. The protocol described in this paper results in the purification of large amounts of stable rTAO with high specific activity. Two factors appeared critical to functionally express highly active rTAO. Firstly, the optimization of culture conditions, including culture duration and IPTG concentration, was crucial for the successful overexpression of rTAO with high specific activity. Secondly, activity was maximized when rTAO was purified from *E. coli* inner membranes—activity decreased substantially when it was isolated from an unpurified membrane fraction. Additionally, changing the detergent from OG to DM following solubilization, also appeared important to maximize yield and activity. Purified rTAO produced in this manner retained complete activity for more than 6 months at 4 °C and for more than 1 month at 20 °C. Furthermore, we have also been able to purify *Sauromattum guttatum* rAOX by this procedure showing the universality of the purification protocol (Elliott, C.E., Kido, Y., Kita, K. and Moore, A.L. unpublished observations).

It is anticipated that highly purified and active AOX will open a new direction with respect to the investigation of the structure and reaction mechanisms of AOXs and contribute to further progress on the study of this novel terminal oxidase. Indeed we recently took advantage of the exceptional stability and purity of the rTAO by performing the first FTIR spectroscopic investigation of any diiron protein [32]. Stepwise reduction of the fully oxidized resting state of rTAO revealed two distinct IR redox difference spectra. The first of these, "signal 1", contained clear features that could be assigned to protonation of at least one carboxylate group, further perturbations of carboxylic and histidine residues, bound ubiquinone and a negative band that might arise from a radical in the fully oxidized protein. A second IR redox difference spectrum, "signal 2", appeared more slowly (within approximately 1 h) once signal 1 had been reduced and is quite distinct from the components which comprise signal 1. The exact identity of the components which result in signal 2 await further investigations. Such a study has not previously been possible with AOX preparations because of protein instability at room temperature.

4.2. Prosthetic group analysis

Prosthetic group analysis summarized in Table 2 revealed that in highly stable and purified rTAO there are two equivalents of iron per rTAO monomer with no other metals, including Cu, Mn and Zn, being detected. EPR spectroscopy confirms that the irons are part of a diiron center since an EPR signal at g = 15 could be detected (Fig. 2) when rTAO is reduced by dithionite in the presence of PMS. The fact that this signal can be detected in all AOXs examined to date suggests that the signal is a characteristic signature of AOXs [30,31] and in agreement with mutational analyses [18,25–29] is further confirmation that TAO, similar to AOXs in other organisms, is a diiron carboxylate protein. Furthermore the data summarized in Table 2 revealed that when the protein was either inactivated or denatured iron was released indicating it is essential for TAO activity. Moreover, this data has established biochemically the validity of predicting the presence of a diiron center from amino acid sequence data, not only in AOX but also in other membrane-bound diiron carboxylate proteins including 5-demethoxyquinone hydroxylase (CLK-1/Coq7) (which also has the diiron binding motif EXXH). It is of interest to note that both AOX and CLK-1/Coq7 utilize ubiquinol as substrate and both are involved in respiration [42–44].

4.3. Kinetic analysis

The inclusion of C10E8 in the assay was found to be critical for the kinetic analysis of TAO and the evaluation of inhibitors. In Table 3, we have calculated fundamental kinetic parameters of TAO and compared them to those of *E. coli* cytochrome *bo* oxidase complex and *S. cerevisiae* ubiquinol–cytochrome *c* reductase [45]. These kinetic constants provide a molecular rationale on how the alternative pathway can effectively compete with other terminal oxidases, although caution must be exercised in the interpretation of this data as it is derived from experiments performed under non-physiological conditions and substrates. Nevertheless Table 3 indicates that TAO has a calculated k_{cat} of $415 \pm 19\ s^{-1}$ (on the basis that the purity of rTAO is 95%), which is slightly higher than that of the cytochrome *bo* oxidase complex ($313\ s^{-1}$), yeast ubiquinol–cytochrome *c* reductase ($153\ s^{-1}$) and previous values reported for the plant AOX ($186\ s^{-1}$), but considerably less than that calculated for cytochrome *c* oxidase ($770\ s^{-1}$) [45–48]. Taking into account that the value of the specificity constant (k_{cat}/K_m) of enzymatic reactions is known to be less than $10^9\ M^{-1}\ s^{-1}$ (from the perspective of diffusion limited access of substrates [49]), it is apparent from Table 3 that both cytochrome *bo* oxidase and TAO have quite high and comparable catalytic activities. These values suggest that the activation energy of both quinol oxidase reactions are similar and furthermore that the quinol oxidase activity of TAO is thermodynamically "alternative" to that of the cytochrome *bo* complex. In contrast however, TAO does not appear to compete effectively with the bc_1 complex in terms of specificity constant and, if the plant AOX possesses a similar specificity constant to that of TAO, it would suggest that plant alternative oxidase activity would be severely curtailed unless the conventional respiratory chain is limited either through inhibition (which appears to be the case under 'stressed conditions') or through down regulation as appears to be the case in thermogenic tissues [12,50,51].

Interestingly ubiquinol-2 oxidation by rTAO showed substrate inhibition at concentrations above 100 μM in a manner similar to that observed when the heterodimeric terminal ubiquinol oxidase of *E. coli*, cytochrome *bd* oxidized ubiquinol-2 as substrate [52]. A lower K_m value of ubiquinol-2 than that of ubiquinol-1 might be related not only to its hydrophobicity but also could be a function of the isoprenoid chain. The peculiar kinetics of ubiquinol-2 might be attributed to the following two points; 1) competition for the ubiquinol-2 oxidation site between the substrate and the product, and 2) the presence of inactive intermediates of the enzyme related to the precise catalytic mechanism.

Kinetic analysis of the mechanism of inhibition by the specific TAO inhibitor ascofuranone (Sup. Fig. 5) indicates that it is a mixed-type inhibitor with respect to ubiquinol-1. The discrepancy between the mixed inhibition observed in this report and competitive inhibition as reported in our previous study [36] might be due to the different assay conditions used in the experiments described in this paper. In the previous study, the kinetic parameters were based on apparent values because enzymatic activity was calculated without detergents and hence only low ranges of ubiquinol-1 concentrations (0.01 K_m–0.3 K_m) could be used. In contrast, the kinetic parameters reported in the current study were determined with much higher reliability since in the presence of C10E8, a much wider range of ubiquinol-1 (0.4 K_m–1.7 K_m) could be used.

Table 3
Kinetic parameters of quinol oxidases (with respect to ubiquinol-1).

	K_m (μM)	V_{max} (μmol/min/mg protein)	k_{cat} (s^{-1})	k_{cat}/K_m ($\mu M^{-1}\ s^{-1}$)
TAO[a]	338 ± 23.2	601 ± 27.0	415 ± 19	1.2
Cyt *bo* oxidase[b]	61	–	313	5.2
Ubiquinol-cyt *c* reductase[c]	13	–	220	16.9

The k_{cat} value of cytochrome *c* oxidase is $k_{cat} = 770\ (s^{-1})$ [46].
All the k_{cat} values listed here were obtained by dividing the V_{max} by the concentration of the enzymes (mol/mg protein).
[a] This study.
[b] *E. coli* cytochrome *bo* oxidase as in Sakamoto et al. [47].
[c] Ubiquinol–cytochrome *c* reductase from bovine heart as in Fato et al. [45].

4.4. Unique feature of AOX

AOX is found in various organisms and recent genome database searches have also identified AOX in different phyla of the Animalia kingdom (Mollusca, Nematoda and Chordata) [17]. It has been suggested that since AOX is absent from mammalian tissues TAO could be a chemotherapeutic target, since it functions in the bloodstream form of *T. brucei* as the only terminal oxidase and hence is essential for the survival of trypanosomes [5,6]. As an AOX protein has also been identified in *Cryptosporidium parvum* [53,54], which causes diarrheal disease cryptosporidiosis, and the recombinant *C. parvum* AOX is also sensitive to ascofuranone and as a result suggests that not only could AOX be a potential drug target in a number of parasites but furthermore ascofuranone could be used to treat a number of infections since this compound shows potent, broad-spectrum antimicrobial activity [53].

In addition to this clinical application, there is considerable interest in the unique characteristics of the enzyme since the functions and properties of TAO are clearly distinct from those of other bacterial quinol oxidases. TAO is a cytochrome-independent and cyanide-insensitive quinol oxidase, whereas cytochrome *bo* and *bd* complexes are cytochrome-dependent and cyanide-sensitive quinol oxidases [34,35]. Furthermore, TAO has various other physiological roles in *T. brucei*; the cytochrome and alternative pathways are both active and functional in the procyclic forms [55] in addition to the bloodstream form, thereby possibly providing metabolic flexibility under changing environmental conditions. TAO activity also appears to regulate the expression of one of the major surface coat proteins, GPEET, in the procyclic form [56], and in addition may regulate the observed programmed cell death-like phenomena in the bloodstream forms [57].

5. Conclusions

The primary aim of our research on TAO is to elucidate the interaction between the enzyme and its substrate or inhibitor, which hopefully could act as a structural guide for ongoing drug development. In addition to the knowledge obtained from this study, further studies on the inhibitory kinetics and structure–activity relationship of ascofuranone derivatives, along with mutational analyses of TAO [27,29] and X-ray structure analysis will undoubtedly have considerable implications with respect to our understanding of how the enzyme interacts with its substrate and inhibitors. A three-dimensional structure of TAO with and without ascofuranone should also shed light on the inhibitory mechanism of this potent drug, which according to this study occurs via a mixed-type inhibition. Such further insights about the interaction between ascofuranone and the enzyme will hopefully lead to a more rational design of more potent and safe anti-trypanosomal drugs.

Acknowledgements

This work was supported in part by Grant-in-aid for Young Scientists (B) 21790402 (to YK), Grant-in-Aid for Scientific Research (C) 21590467 (to YY), Creative Scientific Research Grant 18GS0314 (to KK), Grant-in-aid for Scientific Research on Priority Areas 18073004 (to KK) from the Japanese Society for the Promotion of Science, and Targeted Proteins Research Program (to KK) from the

Japanese Ministry of Education, Science, Culture, Sports and Technology (MEXT) and a grant for research to promote the development of anti-AIDS pharmaceuticals from the Japan Health Sciences Foundation (to KK). ALM gratefully acknowledges BBSRC for financial support and with KK the Prime Ministers Initiative 2 (Connect) fund for collaborative twinning.

Appendix A. Supplementary data

Supplementary data associated with this article can be found, in the online version, at doi:10.1016/j.bbabio.2009.12.021.

References

[1] WHO, Control and surveillance of African trypanosomiasis, Report of a WHO Expert Committee, World Health Organ Tech Rep Ser, vol. 881, 1998, pp. 1–114, I–VI.
[2] C.E. Clayton, P. Michels, Metabolic compartmentation in African trypanosomes, Parasitol. Today 12 (1996) 465–471.
[3] F.R. Opperdoes, P. Borst, S. Bakker, W. Leene, Localization of glycerol-3-phosphate oxidase in the mitochondrion and particulate NAD+-linked glycerol-3-phosphate dehydrogenase in the microbodies of the bloodstream form to *Trypanosoma brucei*, Eur. J. Biochem. 76 (1977) 29–39.
[4] A.B. Clarkson Jr., E.J. Bienen, G. Pollakis, R.W. Grady, Respiration of bloodstream forms of the parasite *Trypanosoma brucei brucei* is dependent on a plant-like alternative oxidase, J. Biol. Chem. 264 (1989) 17770–17776.
[5] M. Chaudhuri, R.D. Ott, G.C. Hill, Trypanosome alternative oxidase: from molecule to function, Trends Parasitol. 22 (2006) 484–491.
[6] C. Nihei, Y. Fukai, K. Kita, Trypanosome alternative oxidase as a target of chemotherapy, Biochim. Biophys. Acta 1587 (2002) 234–239.
[7] N. Minagawa, Y. Yabu, K. Kita, K. Nagai, N. Ohta, K. Meguro, S. Sakajo, A. Yoshimoto, An antibiotic, ascofuranone, specifically inhibits respiration and in vitro growth of long slender bloodstream forms of *Trypanosoma brucei brucei*, Mol. Biochem. Parasitol. 84 (1997) 271–280.
[8] Y. Yabu, A. Yoshida, T. Suzuki, C. Nihei, K. Kawai, N. Minagawa, T. Hosokawa, K. Nagai, K. Kita, N. Ohta, The efficacy of ascofuranone in a consecutive treatment on *Trypanosoma brucei brucei* in mice, Parasitol. Int. 52 (2003) 155–164.
[9] Y. Yabu, T. Suzuki, C. Nihei, N. Minagawa, T. Hosokawa, K. Nagai, K. Kita, N. Ohta, Chemotherapeutic efficacy of ascofuranone in *Trypanosoma vivax*-infected mice without glycerol, Parasitol. Int. 55 (2006) 39–43.
[10] M. Chaudhuri, W. Ajayi, S. Temple, G.C. Hill, Identification and partial purification of a stage-specific 33 kDa mitochondrial protein as the alternative oxidase of the *Trypanosoma brucei brucei* bloodstream trypomastigotes, J. Eukaryot. Microbiol. 42 (1995) 467–472.
[11] A.L. Moore, J.N. Siedow, The regulation and nature of the cyanide-resistant alternative oxidase of plant mitochondria, Biochim. Biophys. Acta 1059 (1991) 121–140.
[12] A.L. Moore, M.S. Albury, Further insights into the structure of the alternative oxidase: from plants to parasites, Biochem. Soc. Trans. 36 (2008) 1022–1026.
[13] J.N. Siedow, A.L. Umbach, The mitochondrial cyanide-resistant oxidase: structural conservation amid regulatory diversity, Biochim. Biophys. Acta 1459 (2000) 432–439.
[14] T. Joseph-Horne, D.W. Hollomon, P.M. Wood, Fungal respiration: a fusion of standard and alternative components, Biochim. Biophys. Acta 1504 (2001) 179–195.
[15] A. McDonald, G. Vanlerberghe, Branched mitochondrial electron transport in the Animalia: presence of alternative oxidase in several animal phyla, IUBMB Life 56 (2004) 333–341.
[16] A.E. McDonald, G.C. Vanlerberghe, Alternative oxidase and plastoquinol terminal oxidase in marine prokaryotes of the Sargasso Sea, Gene 349 (2005) 15–24.
[17] A.E. McDonald, G.C. Vanlerberghe, J.F. Staples, Alternative oxidase in animals: unique characteristics and taxonomic distribution, J. Exp. Biol. 212 (2009) 2627–2634.
[18] D.A. Berthold, M.E. Andersson, P. Nordlund, New insight into the structure and function of the alternative oxidase, Biochim. Biophys. Acta 1460 (2000) 241–254.
[19] C. Affourtit, M.S. Albury, P.G. Crichton, A.L. Moore, Exploring the molecular nature of alternative oxidase regulation and catalysis, FEBS Lett. 510 (2002) 121–126.
[20] D.P. Maxwell, Y. Wang, L. McIntosh, The alternative oxidase lowers mitochondrial reactive oxygen production in plant cells, Proc. Natl. Acad. Sci. U. S. A. 96 (1999) 8271–8276.
[21] A.L. Moore, M.S. Albury, P.G. Crichton, C. Affourtit, Function of the alternative oxidase: is it still a scavenger? Trends Plant Sci. 7 (2002) 478–481.
[22] S. Mackenzie, L. McIntosh, Higher plant mitochondria, Plant Cell 11 (1999) 571–586.
[23] J.N. Siedow, A.L. Umbach, A.L. Moore, The active site of the cyanide-resistant oxidase from plant mitochondria contains a binuclear iron center, FEBS Lett. 362 (1995) 10–14.
[24] M.E. Andersson, P. Nordlund, A revised model of the active site of alternative oxidase, FEBS Lett. 449 (1999) 17–22.
[25] M.S. Albury, C. Affourtit, A.L. Moore, A highly conserved glutamate residue (Glu-270) is essential for plant alternative oxidase activity, J. Biol. Chem. 273 (1998) 30301–30305.
[26] M. Chaudhuri, W. Ajayi, G.C. Hill, Biochemical and molecular properties of the *Trypanosoma brucei* alternative oxidase, Mol. Biochem. Parasitol. 95 (1998) 53–68.
[27] W.U. Ajayi, M. Chaudhuri, G.C. Hill, Site-directed mutagenesis reveals the essentiality of the conserved residues in the putative diiron active site of the trypanosome alternative oxidase, J. Biol. Chem. 277 (2002) 8187–8193.
[28] M.S. Albury, C. Affourtit, P.G. Crichton, A.L. Moore, Structure of the plant alternative oxidase. Site-directed mutagenesis provides new information on the active site and membrane topology, J. Biol. Chem. 277 (2002) 1190–1194.
[29] K. Nakamura, K. Sakamoto, Y. Kido, Y. Fujimoto, T. Suzuki, M. Suzuki, Y. Yabu, N. Ohta, A. Tsuda, M. Onuma, K. Kita, Mutational analysis of the *Trypanosoma vivax* alternative oxidase: the $E(X)_6Y$ motif is conserved in both mitochondrial alternative oxidase and plastid terminal oxidase and is indispensable for enzyme activity, Biochem. Biophys. Res. Commun. 334 (2005) 593–600.
[30] D.A. Berthold, N. Voevodskaya, P. Stenmark, A. Graslund, P. Nordlund, EPR studies of the mitochondrial alternative oxidase. Evidence for a diiron carboxylate center, J. Biol. Chem. 277 (2002) 43608–43614.
[31] A.L. Moore, J.E. Carre, C. Affourtit, M.S. Albury, P.G. Crichton, K. Kita, P. Heathcote, Compelling EPR evidence that the alternative oxidase is a diiron carboxylate protein, Biochim. Biophys. Acta 1777 (2008) 327–330.
[32] A. Maréchal, Y. Kido, K. Kita, A.L. Moore, P.R. Rich, Identification of three redox states of recombinant *Trypanosoma brucei* alternative oxidase by FTIR spectroscopy and electrochemistry, J. Biol. Chem. 284 (2009) 31827–31833.
[33] Y. Fukai, H. Amino, H. Hirawake, Y. Yabu, N. Ohta, N. Minagawa, S. Sakajo, A. Yoshimoto, K. Nagai, S. Takamiya, S. Kojima, K. Kita, Functional expression of the ascofuranone-sensitive *Trypanosoma brucei brucei* alternative oxidase in the cytoplasmic membrane of *Escherichia coli*, Comp. Biochem. Physiol. C Pharmacol. Toxicol. Endocrinol. 124 (1999) 141–148.
[34] K. Kita, K. Konishi, Y. Anraku, Terminal oxidases of *Escherichia coli* aerobic respiratory chain. I. Purification and properties of cytochrome b_{562}–*o* complex from cells in the early exponential phase of aerobic growth, J. Biol. Chem. 259 (1984) 3368–3374.
[35] K. Kita, K. Konishi, Y. Anraku, Terminal oxidases of *Escherichia coli* aerobic respiratory chain. II. Purification and properties of cytochrome b_{558}–*d* complex from cells grown with limited oxygen and evidence of branched electron-carrying systems, J. Biol. Chem. 259 (1984) 3375–3381.
[36] C. Nihei, Y. Fukai, K. Kawai, A. Osanai, Y. Yabu, T. Suzuki, N. Ohta, N. Minagawa, K. Nagai, K. Kita, Purification of active recombinant trypanosome alternative oxidase, FEBS Lett. 538 (2003) 35–40.
[37] O. Maglio, F. Nastri, V. Pavone, A. Lombardi, W.F. DeGrado, Preorganization of molecular binding sites in designed diiron proteins, Proc. Natl. Acad. Sci. U. S. A. 100 (2003) 3772–3777.
[38] M.P. Hendrich, E. Munck, B.G. Fox, J.D. Lipscomb, Integer-spin Epr studies of the fully reduced methane monooxygenase hydroxylase component, J. Am. Chem. Soc. 112 (1990) 5861–5865.
[39] W.A. van den Berg, A.A. Stevens, M.F. Verhagen, W.M. van Dongen, W.R. Hagen, Overproduction of the prismane protein from *Desulfovibrio desulfuricans* ATCC 27774 in *Desulfovibrio vulgaris* (Hildenborough) and EPR spectroscopy of the [6Fe–6S] cluster in different redox states, Biochim. Biophys. Acta 1206 (1994) 240–246.
[40] M. Hoefnagel, P.R. Rich, Q. Zhang, J.T. Wiskich, Substrate kinetics of the plant mitochondrial alternative oxidase and the effects of pyruvate, Plant Physiol. 115 (1997) 1145–1153.
[41] Y. Kido, T. Shiba, D.K. Inaoka, K. Sakamoto, T. Nara, T. Aoki, T. Honma, A. Tanaka, M. Inoue, S. Matsuoka, A. Moore, S. Harada, K. Kita, Crystallization and preliminary crystallographic analysis of cyanide-insensitive alternative oxidase from *Trypanosoma brucei brucei*, Acta. Crystallogr. Sect. F Struct. Biol. Cryst. Commun, doi:10.1107/S1744309109054062.
[42] H. Miyadera, H. Amino, A. Hiraishi, H. Taka, K. Murayama, H. Miyoshi, K. Sakamoto, N. Ishii, S. Hekimi, K. Kita, Altered quinone biosynthesis in the long-lived clk-1 mutants of *Caenorhabditis elegans*, J. Biol. Chem. 276 (2001) 7713–7716.
[43] P. Stenmark, J. Grunler, J. Mattsson, P.J. Sindelar, P. Nordlund, D.A. Berthold, A new member of the family of di-iron carboxylate proteins. Coq7 (clk-1), a membrane-bound hydroxylase involved in ubiquinone biosynthesis, J. Biol. Chem. 276 (2001) 33297–33300.
[44] D.A. Berthold, P. Stenmark, Membrane-bound diiron carboxylate proteins, Ann. Rev. Plant Biol. 54 (2003) 497–517.
[45] R. Fato, M. Cavazzoni, C. Castelluccio, G. Parenti Castelli, G. Palmer, M. Degli Esposti, G. Lenaz, Steady-state kinetics of ubiquinol–cytochrome *c* reductase in bovine heart submitochondrial particles: diffusional effects, Biochem. J. 290 (1993) 225–236 K.
[46] H. Witt, F. Malatesta, F. Nicoletti, M. Brunori, B. Ludwig, Tryptophan 121 of subunit II is the electron entry site to cytochrome-*c* oxidase in *Paracoccus denitrificans*. Involvement of a hydrophobic patch in the docking reaction, J. Biol. Chem. 273 (1998) 5132–5136.
[47] Sakamoto, H. Miyoshi, M. Ohshima, K. Kuwabara, K. Kano, T. Akagi, T. Mogi, H. Iwamura, Role of the isoprenyl tail of ubiquinone in reaction with respiratory enzymes: studies with bovine heart mitochondrial complex I and *Escherichia coli bo*-type ubiquinol oxidase, Biochemistry 37 (1998) 15106–15113.
[48] M.H.N. Hoefnagel, J.T. Wiskich, S.A. Madgwick, Z. Patterson, W. Oettmeier, P.R. Rich New, Inhibitors of the ubiquinol oxidase of higher plant mitochondria, Eur. J. Biochem. 233 (1995) 531–537.
[49] R.A. Alberty, G.G. Hammes, Application of the theory of diffusion-controlled reactions to enzyme kinetics, J. Phys. Chem. 62 (1958) 154–159.
[50] R. Clifton, A.H. Millar, J. Whelan, Alternative oxidases in Arabidopsis: a comparative analysis of differential expression in the gene family provides new insights into function of non-phosphorylating bypasses, Biochim. Biophys. Acta 1757 (2006) 730–741.
[51] A.M. Wagner, K. Krab, M.J. Wagner, A.L. Moore, Regulation of thermogenesis in flowering Araceae: the role of the alternative oxidase, Biochim. Biophys. Acta 1777 (2008) 993–1000.

[52] K. Sakamoto, H. Miyoshi, K. Takegami, T. Mogi, Y. Anraku, H. Iwamura, Probing substrate binding site of the *Escherichia coli* quinol oxidases using synthetic ubiquinol analogues, J. Biol. Chem. 271 (1996) 29897–29902.
[53] T. Suzuki, T. Hashimoto, Y. Yabu, Y. Kido, K. Sakamoto, C. Nihei, M. Hato, S. Suzuki, Y. Amano, K. Nagai, T. Hosokawa, N. Minagawa, N. Ohta, K. Kita, Direct evidence for cyanide-insensitive quinol oxidase (alternative oxidase) in apicomplexan parasite *Cryptosporidium parvum*: phylogenetic and therapeutic implications, Biochem. Biophys. Res. Commun. 313 (2004) 1044–1052.
[54] C.W. Roberts, F. Roberts, F.L. Henriquez, D. Akiyoshi, B.U. Samuel, T.A. Richards, W. Milhous, D. Kyle, L. McIntosh, G.C. Hill, M. Chaudhuri, S. Tzipori, R. McLeod, Evidence for mitochondrial-derived alternative oxidase in the apicomplexan parasite *Cryptosporidium parvum*: a potential anti-microbial agent target, Int. J. Parasitol. 34 (2004) 297–308.
[55] R. Walker Jr., L. Saha, G.C. Hill, M. Chaudhuri, The effect of over-expression of the alternative oxidase in the procyclic forms of *Trypanosoma brucei*, Mol. Biochem. Parasitol. 139 (2005) 153–162.
[56] E. Vassella, M. Probst, A. Schneider, E. Studer, C.K. Renggli, I. Roditi, Expression of a major surface protein of *Trypanosoma brucei* insect forms is controlled by the activity of mitochondrial enzymes, Mol. Biol. Cell 15 (2004) 3986–3993.
[57] A. Tsuda, W.H. Witola, K. Ohashi, M. Onuma, Expression of alternative oxidase inhibits programmed cell death-like phenomenon in bloodstream form of *Trypanosoma brucei rhodesiense*, Parasitol. Int. 54 (2005) 243–251.

Acta Crystallographica Section F
Structural Biology and Crystallization Communications
ISSN 1744-3091
Editors: **H. M. Einspahr and M. S. Weiss**

Crystallization and preliminary crystallographic analysis of cyanide-insensitive alternative oxidase from *Trypanosoma brucei brucei*

Yasutoshi Kido, Tomoo Shiba, Daniel Ken Inaoka, Kimitoshi Sakamoto, Takeshi Nara, Takashi Aoki, Teruki Honma, Akiko Tanaka, Masayuki Inoue, Shigeru Matsuoka, Anthony Moore, Shigeharu Harada and Kiyoshi Kita

Acta Cryst. (2010). F**66**, 275–278

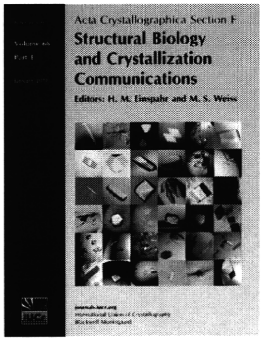

Acta Crystallographica Section F: Structural Biology and Crystallization Communications is a rapid all-electronic journal, which provides a home for short communications on the crystallization and structure of biological macromolecules. It includes four categories of publication: protein structure communications; nucleic acid structure communications; structural genomics communications; and crystallization communications. Structures determined through structural genomics initiatives or from iterative studies such as those used in the pharmaceutical industry are particularly welcomed. *Section F* is essential for all those interested in structural biology including molecular biologists, biochemists, crystallization specialists, structural biologists, biophysicists, pharmacologists and other life scientists.

Acta Crystallographica Section F
Structural Biology and Crystallization Communications
ISSN 1744-3091

Crystallization and preliminary crystallographic analysis of cyanide-insensitive alternative oxidase from *Trypanosoma brucei brucei*

Yasutoshi Kido,[a] Tomoo Shiba,[a] Daniel Ken Inaoka,[a] Kimitoshi Sakamoto,[a] Takeshi Nara,[b] Takashi Aoki,[b] Teruki Honma,[c] Akiko Tanaka,[c] Masayuki Inoue,[d] Shigeru Matsuoka,[d] Anthony Moore,[e] Shigeharu Harada[f]* and Kiyoshi Kita[a]*

[a]Department of Biomedical Chemistry, Graduate School of Medicine, The University of Tokyo, Tokyo 113-0033, Japan, [b]Department of Molecular and Cellular Parasitology, Juntendo University School of Medicine, Tokyo 113-8421, Japan, [c]Systems and Structural Biology Center, RIKEN, Tsurumi, Yokohama 230-0045, Japan, [d]Graduate School of Pharmaceutical Sciences, The University of Tokyo, Tokyo 113-0033, Japan, [e]Biochemistry and Biomedical Sciences, School of Life Sciences, University of Sussex, Falmer, Brighton, England, and [f]Department of Applied Biology, Graduate School of Science and Technology, Kyoto Institute of Technology, Kyoto 606-8585, Japan

Correspondence e-mail: harada@kit.ac.jp, kitak@m.u-tokyo.ac.jp

Received 6 September 2009
Accepted 15 December 2009

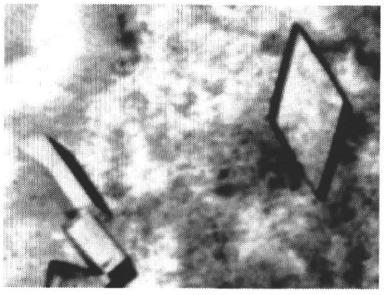

Cyanide-insensitive alternative oxidase (AOX) is a mitochondrial membrane protein and a non-proton-pumping ubiquinol oxidase that catalyzes the four-electron reduction of dioxygen to water. In the African trypanosomes, trypanosome alternative oxidase (TAO) functions as a cytochrome-independent terminal oxidase that is essential for survival in the mammalian host; hence, the enzyme is considered to be a promising drug target for the treatment of trypanosomiasis. In the present study, recombinant TAO (rTAO) overexpressed in haem-deficient *Escherichia coli* was purified and crystallized at 293 K by the hanging-drop vapour-diffusion method using polyethylene glycol 400 as a precipitant. X-ray diffraction data were collected at 100 K and were processed to 2.9 Å resolution with 93.1% completeness and an overall $R_{\rm merge}$ of 9.5%. The TAO crystals belonged to the orthorhombic space group $I222$ or $I2_12_12_1$, with unit-cell parameters $a = 63.11$, $b = 136.44$, $c = 223.06$ Å. Assuming the presence of two rTAO molecules in the asymmetric unit (2 × 38 kDa), the calculated Matthews coefficient ($V_{\rm M}$) was 3.2 Å^3 Da^{-1}, which corresponds to a solvent content of 61.0%. This is the first report of a crystal of the membrane-bound diiron proteins, which include AOXs.

1. Introduction

Cyanide-insensitive respiration in plants has been recognized since the 1920s (Moore & Siedow, 1991). Intensive biochemical studies have revealed that the mitochondrial membrane enzyme alternative oxidase (AOX) is responsible for cyanide-insensitive respiration (Moore & Siedow, 1991; Siedow & Umbach, 2000; Moore & Albury, 2008). AOX, which is cyanide-insensitive and sensitive to salicyl hydroxamic acid (SHAM), is a non-proton-pumping ubiquinol oxidase that catalyzes the four-electron reduction of dioxygen to water (Moore & Albury, 2008). AOX has been found in higher plants, algae, yeast, slime moulds, free-living amoebae, eubacteria and nematodes, as well as in protozoa, including trypanosomes (McDonald *et al.*, 2009).

Trypanosoma brucei, which causes African sleeping sickness in humans and nagana in livestock, which are serious health and economic problems in sub-Saharan Africa (World Health Organization, 2006), is known to show cyanide-insensitive respiration (Opperdoes *et al.*, 1977; Chaudhuri *et al.*, 2006). In the African trypanosomes, trypanosome alternative oxidase (TAO) functions in cyanide-insensitive respiration as a cytochrome-independent terminal oxidase (Clarkson *et al.*, 1989) that is essential for survival in the mammalian host (Clayton & Michels, 1996; Chaudhuri *et al.*, 2006).

TAO is thought to be a good target for antitrypanosomal drugs because mammalian hosts do not possess this protein (Nihei *et al.*, 2002; Chaudhuri *et al.*, 2006). Indeed, we found that ascofuranone, which is isolated from the pathogenic fungus *Ascochyta visiae*, specifically inhibits the quinol oxidase activity of TAO (Minagawa *et al.*, 1997) and rapidly kills the parasites. In addition, we have confirmed the chemotherapeutic efficacy of ascofuranone *in vivo* (Yabu *et al.*, 2003, 2006).

Although TAO and other alternative oxidases (AOXs) contain diiron-binding motifs (E*XX*H) in their amino-acid sequences, their three-dimensional structures have not yet been elucidated (Berthold

& Stenmark, 2003; Moore & Albury, 2008). The high-resolution structure of TAO will undoubtedly have considerable implications with respect to their physicochemical mechanism, enzyme reaction and structure–function relationship, including the interaction between the enzyme and ascofuranone, which may lead to the rational design of more potent and safer antitrypanosomal drugs. Here, we describe the crystallization and preliminary crystallographic analysis of TAO.

2. Materials and methods

2.1. Preparation of rTAO

To construct the host strain FN102 for the expression of rTAO, the Δ*hemA*::Km^R mutation was introduced into *Escherichia coli* strain BL21 (DE3) by P1 transduction as described in a previous study (Nihei *et al.*, 2003). The strain FN102/pTbAO (Nihei *et al.*, 2003) carrying the cDNA for *T. brucei brucei* TAO was precultured at 310 K in 100 ml LB medium (containing 10 mg ampicillin, 5 mg kanamycin and 5 mg 5-aminolevulinic acid) for 4–6 h. The precultured cells were grown aerobically at 303 K in 10 l S-medium [100 g tryptone peptone, 50 g yeast extract, 50 g casamino acids, 104 g K_2HPO_4, 30 g KH_2PO_4, 7.5 g trisodium citrate.$2H_2O$, 25 g $(NH_4)_2SO_4$, 0.5 g $MgSO_4.7H_2O$, 0.25 g $FeSO_4.7H_2O$, 0.25 g $FeCl_3$, 20 g glucose and 0.1 g carbenicillin]. The culture was started at an OD_{600} of 0.01 and expression of His_6-tagged rTAO was induced by the addition of isopropyl β-D-1-thiogalactopyranoside (IPTG; 25 μ*M*) when the OD_{600} reached 0.1. The cells were harvested 8–10 h after induction (about 40 g wet weight). The cells were then resuspended in 200 ml 50 m*M* Tris–HCl pH 7.5 containing 20%(*w*/*w*) sucrose, 0.1 m*M* phenylmethanesulfonylfluoride and protease inhibitor cocktail (Sigma) and broken using a French pressure cell at 200 MPa (Ohtake, Tokyo). Unbroken cells were removed as a pellet by centrifugation at 8000*g* for 10 min (Hitachi 21G). The supernatant (35 ml) was loaded onto 35 ml 50 m*M* Tris–HCl pH 7.5 containing 40%(*w*/*w*) sucrose and ultracentrifuged at 200 000*g* for 1 h at 277 K (Hitachi 85H); the fraction of inner membranes buoyant on the 40%(*w*/*w*) sucrose layer was recovered. The inner-membrane pellet was separated by further ultracentrifugation at 200 000*g* for 1 h (Hitachi 85H) and was resuspended in 30 ml 50 m*M* Tris–HCl pH 7.5 containing 20%(*w*/*w*) sucrose. To solubilize rTAO from the membranes, the membrane suspension (35 ml) was diluted with buffer [50 m*M* Tris–HCl, 200 m*M* $MgSO_4$, 20%(*v*/*v*) glycerol pH 7.3] at 277 K to give a 6 mg ml^{-1} solution and 14%(*w*/*v*) *n*-octyl β-D-glucopyranoside (OG) was added to a final concentration of 1.4%(*w*/*v*). The solution was immediately ultracentrifuged at 200 000*g* for 1 h at 277 K to recover the supernatant containing the solubilized rTAO.

Cobalt-affinity chromatography was performed by a hybrid batch/column procedure using the manufacturer's instructions as stated below. 10 ml BD TALON Metal Affinity Resin (BD Bioscience) equilibrated in a batch format with 100 ml equilibration buffer [20 m*M* Tris–HCl, 1.4%(*w*/*v*) OG, 100 m*M* $MgSO_4$, 20%(*v*/*v*) glycerol pH 7.3] was mixed with 20 ml of the OG extract for 20 min at 277 K. The resin was washed twice with 100 ml of the first wash buffer [20 m*M* Tris–HCl, 20 m*M* imidazole, 0.042%(*w*/*v*) *n*-dodecyl β-D-maltopyranoside (DM), 50 m*M* $MgSO_4$, 20%(*v*/*v*) glycerol pH 7.3] and then transferred to a column for additional washing with 20 ml of the second wash buffer [20 m*M* Tris–HCl, 165 m*M* imidazole, 0.042%(*w*/*v*) DM, 50 m*M* $MgSO_4$, 20%(*v*/*v*) glycerol pH 7.3; flow rate 1 ml min^{-1}]. After washing, rTAO was eluted with elution buffer [20 m*M* Tris–HCl, 200 m*M* imidazole, 0.042%(*w*/*v*) DM, 50 m*M* $MgSO_4$, 60 m*M* NaCl, 20%(*v*/*v*) glycerol pH 7.3; flow rate 1 ml min^{-1}] and the fractions containing rTAO as judged by activity measurements and SDS–PAGE were pooled (Kido *et al.*, 2010).

The fused N-terminal His_6 tag was removed from the purified rTAO using biotinylated thrombin and the tag-free rTAO was separated using streptavidin agarose (Biotinylated Thrombin Cleavage Capture Kit, Novagen) according to the manufacturer's instructions. Incubation with 10 U thrombin for 16 h at 293 K was required for the complete cleavage of 10 mg protein.

The molecular weight of the enzyme in solution was estimated by gel-filtration chromatography using a HiLoad 16/60 Superdex 200 pg column (GE Healthcare). Elution was carried out at a flow rate of 0.3 ml min^{-1} using 50 m*M* Tris–HCl pH 7.4, 0.1 *M* NaCl, 0.042%(*w*/*v*) DM and 20%(*v*/*v*) glycerol.

2.2. Crystallization and X-ray data collection

The purified rTAO was concentrated to 5 mg ml^{-1} in 20 m*M* Tris–HCl, 0.042%(*w*/*v*) DM, 50 m*M* $MgSO_4$, 20%(*v*/*v*) glycerol pH 7.3 using an Amicon Ultra centrifugal filter device (Millipore, 30 kDa molecular-weight cutoff) and used for initial screening of crystallization conditions. Crystallization was performed by the sitting-drop vapour-diffusion technique in 96-well Corning CrystalEX microplates with a conical flat bottom (Hampton Research). In the screening, 0.5 μl rTAO solution was mixed with an equal volume of reservoir solution and the droplet was equilibrated against 100 μl reservoir solution at 277 and 293 K. Commercially available screening kits purchased from Hampton Research (Crystal Screen, Crystal Screen II, Crystal Screen Lite, SaltRx and MembFac), Emerald BioStructures (Wizard I, Wizard II, Cryo I and Cryo II) and Fluidigm (OptiMax-5 Membrane), together with homemade grid-screen reagents containing 100 m*M* buffer (pH 5.0–9.0), 10–40%(*w*/*v*) polyethylene glycol (PEG 400, PEG 1000, PEG 3350, PEG 6000 and PEG 10 000) and 200 m*M* salts (NaCl and KCl), were used as reservoir solutions. However, crystals of rTAO did not appear.

Subsequently, screening was carried out at 277 K using various detergents (DM, OG, *n*-decyl β-D-maltopyranoside, *n*-octyl β-D-maltopyranoside, *n*-nonanoyl *N*-methyl-D-glucamine, octaethylene glycol monododecylether, tetraethylene glycol monooctylether and hexaethylene glycol monodecylether). rTAO samples dissolved in different detergents were subjected to free-interface diffusion in a TOPAZ 8.96 Screening Tip against reservoir solutions purchased from TOPAZ (OptiMax-1, OptiMax-2, OptiMax-3, OptiMax-4 PEG and OptiMax-5 Membrane) using a Fluidigm TOPAZ system (Segelke, 2005). When OG was used as a detergent, several reservoir solutions containing low-molecular-weight PEGs as precipitants gave tiny crystals. The conditions were further optimized by varying the PEG (PEG 200, PEG 400 and PEG 1000) concentration (10–40%), the buffer pH (6.0–8.0), the salt type (48 salts found in PEG/Ion Screen kit from Hampton Research) and the temperature (277 and 293 K) using the sitting-drop vapour-diffusion method. However, crystals larger than 30 μm could not be obtained and moreover they only diffracted X-rays to 7 Å resolution at most.

Next, the effects of additive detergents on crystal growth and X-ray diffraction were examined using reservoir solutions [25–40%(*w*/*v*) PEG 400, 100 m*M* imidazole buffer pH 6.2–7.8 and 200 m*M* potassium formate] supplemented with 0.1–0.5%(*w*/*v*) additive detergents. A dramatic improvement in crystal size was achieved using tetraethylene glycol monooctylether (C8E4) and the conditions, including the concentration of C8E4, were finally optimized.

Currently, crystals with average dimensions of approximately 0.1 × 0.07 × 0.03 mm can be reproducibly obtained at 293 K from reservoir solution consisting of 28–34%(*w*/*v*) PEG 400, 100 m*M*

imidazole buffer pH 7.4, 500 m*M* potassium formate and 0.4%(*w*/*v*) C8E4 using rTAO dissolved in 20 m*M* Tris–HCl pH 7.3, 0.8%(*w*/*v*) OG, 20 m*M* $MgSO_4$ and 20%(*v*/*v*) glycerol.

X-ray diffraction experiments were performed using synchrotron radiation on BL44XU and BL41XU at SPring-8 (Harima, Japan), BL5A and BL17A at Photon Factory and NW12A at Photon Factory Advanced Ring (Tsukuba, Japan). A crystal mounted in a nylon loop was frozen by rapidly submerging it in liquid nitrogen and X-ray diffraction patterns were recorded at 100 K. The best crystals diffracted X-rays to better than 3.0 Å resolution and a total of 180 images were recorded with an oscillation angle of 1°, an exposure time of 5 s per image and a crystal-to-detector distance of 280 mm. The data were processed and scaled using the *HKL*-2000 software package (Otwinowski & Minor, 1997).

3. Results and discussion

His_6-tagged rTAO was solubilized from inner membranes using OG and was purified by cobalt-affinity chromatography in the presence of DM. After removal of the fused N-terminal His_6 tag, about 10 mg of enzyme was obtained from a 10 l culture. The purified rTAO, consisting of 329 amino-acid residues (38 kDa), was >95% pure as estimated by SDS–PAGE (Fig. 1) and its molecular weight in solution was estimated to be 110 kDa by gel-filtration chromatography. As rTAO was prepared as a water-soluble rTAO–DM complex, the complex is probably composed of a homodimer of rTAO with DM molecules bound to the hydrophobic surface of the homodimer. A homodimeric structure of TAO has also been suggested by Chaudhuri *et al.* (2005). The molecular weight of the rTAO–OG complex could not be estimated because elution of rTAO from the gel-filtration column was only successful in the presence of DM as a detergent.

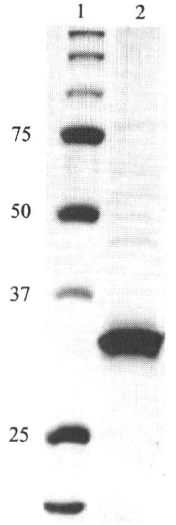

Figure 1
12.5% SDS–PAGE of rTAO with Coomassie Brilliant Blue R-250 staining. Lane 1, molecular-weight markers (kDa); lane 2, rTAO purified by affinity chromatography using BD TALON Metal Affinity Resin.

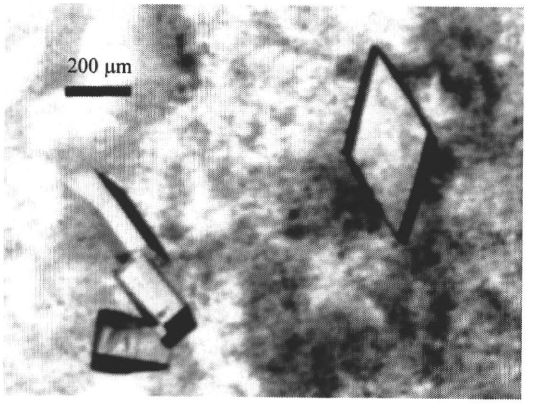

Figure 2
Rhombic plate-shaped crystals of rTAO obtained by the sitting-drop vapour-diffusion method using PEG 400 as a precipitant.

Table 1
Diffraction data statistics.

Values in parentheses are for the outermost resolution shell.

Space group	*I*222 or $I2_12_12_1$
Unit-cell parameters (Å)	a = 63.11, b = 136.44, c = 223.06
Beamline	SPring-8 BL41XU
Wavelength (Å)	1.000
Temperature (K)	100
Resolution (Å)	50.0– 2.90 (2.95–2.90)
Total reflections	135535
Unique reflections	21720
Completeness (%)	93.1 (63.2)
$R_{merge}(I)$† (%)	9.5 (57.3)
$\langle I/\sigma(I)\rangle$	9.8 (1.7)

† $R_{merge}(I) = \sum_{hkl}\sum_i |I_i(hkl) - \langle I(hkl)\rangle| / \sum_{hkl}\sum_i I_i(hkl)$, where $I_i(hkl)$ is the ith measurement of reflection hkl.

After extensive screening and optimization of crystallization conditions, crystals with average dimensions of approximately 0.1 × 0.07 × 0.03 mm could be obtained within 10 d at 293 K using rTAO dissolved in 20 m*M* Tris–HCl pH 7.3, 0.8%(*w*/*v*) OG, 20 m*M* $MgSO_4$ and 20%(*v*/*v*) glycerol with a reservoir solution containing 28–34%(*w*/*v*) PEG 400, 100 m*M* imidazole buffer pH 7.4, 100 m*M* potassium formate and 0.4%(*w*/*v*) C8E4 (Fig. 2).

Analyses of the symmetry and systematic absences in the recorded diffraction patterns indicated that the crystals belonged to the orthorhombic space group *I*222 or $I2_12_12_1$, with unit-cell parameters a = 63.11, b = 136.44, c = 223.06 Å. Assuming the presence of two rTAO molecules in the asymmetric unit (2 × 38 kDa), the calculated Matthews coefficient (V_M) is 3.2 $Å^3\ Da^{-1}$, which corresponds to a solvent content of 61.0%. If the molecular weight of the rTAO–OG complex is presumed to be comparable to that of the rTAO–DM complex, the presence of one molecule of the rTAO–OG complex in the asymmetric unit gives a V_M value of 2.2 $Å^3\ Da^{-1}$ and a solvent content of 44.1%. A data set to 2.9 Å resolution (21 720 unique reflections) was obtained after merging 135 535 reflections recorded on 180 images, with 93.1% completeness and an overall R_{merge} of 9.5%. Statistics of data collection and processing are shown in Table 1. Currently, data collection for phasing using the anomalous dispersion effect of iron is in progress. This is the first report of the crystallization of membrane-bound diiron proteins, which include AOXs.

We thank all staff members of beamlines BL44XU and BL41XU at SPring-8, BL5A and BL17A at Photon Factory and NW12 at Photon Factory Advanced Ring for their help with X-ray diffraction data collection. This work was supported in part by grant-in-aid for Young Scientists (B) 21790402 (to YK), Creative Scientific Research Grant 18GS0314 (to KK), grant-in-aid for Scientific Research on Priority Areas 18073004 (to KK) from the Japanese Society for the Promotion of Science and the Targeted Proteins Research Program (to KK) of the Japanese Ministry of Education, Science, Culture, Sports and Technology (MEXT). ALM gratefully acknowledges the BBSRC for

financial support and, together with KK, the Prime Minister's Initiative 2 (Connect) fund for collaborative twinning.

References

Berthold, D. A. & Stenmark, P. (2003). *Annu. Rev. Plant Biol.* **54**, 497–517.
Chaudhuri, M., Ott, R. D. & Hill, G. C. (2006). *Trends Parasitol.* **22**, 484–491.
Chaudhuri, M., Ott, R. D., Saha, L., Williams, S. & Hill, G. C. (2005). *Parasitol. Res.* **96**, 178–183.
Clarkson, A. B. Jr, Bienen, E. J., Pollakis, G. & Grady, R. W. (1989). *J. Biol. Chem.* **264**, 17770–17776.
Clayton, C. E. & Michels, P. (1996). *Parasitol. Today*, **12**, 465–471.
Kido, Y., Sakamoto, K., Nakamura, K., Harada, M., Suzuki, T., Yabu, Y., Saimoto, H., Yamakura, F., Ohmori, D., Moore, A., Harada, S. & Kita, K., (2010). *Biochim. Biophys. Acta*, doi:10.1016/j.bbabio.2009.12.021.
McDonald, A. E., Vanlerberghe, G. C. & Staples, J. F. (2009). *J. Exp. Biol.* **212**, 2627–2634.
Minagawa, N., Yabu, Y., Kita, K., Nagai, K., Ohta, N., Meguro, K., Sakajo, S. & Yoshimoto, A. (1997). *Mol. Biochem. Parasitol.* **84**, 271–280.
Moore, A. L. & Albury, M. S. (2008). *Biochem. Soc. Trans.* **36**, 1022–1026.
Moore, A. L. & Siedow, J. N. (1991). *Biochim. Biophys. Acta*, **1059**, 121–140.
Nihei, C., Fukai, Y., Kawai, K., Osanai, A., Yabu, Y., Suzuki, T., Ohta, N., Minagawa, N., Nagai, K. & Kita, K. (2003). *FEBS Lett.* **538**, 35–40.
Nihei, C., Fukai, Y. & Kita, K. (2002). *Biochim. Biophys. Acta*, **1587**, 234–239.
Opperdoes, F. R., Borst, P., Bakker, S. & Leene, W. (1977). *Eur. J. Biochem.* **76**, 29–39.
Otwinowski, Z. & Minor, W. (1997). *Methods Enzymol.* **276**, 307–326.
Segelke, B. (2005). *Expert Rev. Proteomics*, **2**, 165–172.
Siedow, J. N. & Umbach, A. L. (2000). *Biochim. Biophys. Acta*, **1459**, 432–439.
World Health Organization (2006). *Wkly Epidemiol. Rec.* **81**, 71–80.
Yabu, Y., Suzuki, T., Nihei, C., Minagawa, N., Hosokawa, T., Nagai, K., Kita, K. & Ohta, N. (2006). *Parasitol. Int.* **55**, 39–43.
Yabu, Y., Yoshida, A., Suzuki, T., Nihei, C., Kawai, K., Minagawa, N., Hosokawa, T., Nagai, K., Kita, K. & Ohta, N. (2003). *Parasitol. Int.* **52**, 155–164.

Molecular Biology and Evolution

Divergence of the Mitochondrial Genome Structure in the Apicomplexan Parasites, Babesia and Theileria

Kenji Hikosaka,[1] Yoh-ichi Watanabe,[2] Naotoshi Tsuji,[3] Kiyoshi Kita,[2] Hiroe Kishine,[4] Nobuko Arisue,[5] Nirianne Marie Q. Palacpac,[5] Shin-ichiro Kawazu,[6] Hiromi Sawai,[1] Toshihiro Horii,[5] Ikuo Igarashi,[6] and Kazuyuki Tanabe[1,*]

[1]Laboratory of Malariology, International Research Center of Infectious Diseases, Research Institute for Microbial Diseases, Osaka University, Suita, Osaka, Japan

[2]Department of Biomedical Chemistry, Graduate School of Medicine, The University of Tokyo, Bunkyo-ku, Tokyo, Japan

[3]Laboratory of Parasitic Diseases, National Institute of Animal Health, National Agriculture and Food Research Organization, Tsukuba, Ibaraki, Japan

[4]Department of Molecular Biology, Research Institute for Microbial Diseases, Osaka University, Suita, Osaka, Japan

[5]Department of Molecular Protozoology, Research Institute for Microbial Diseases, Osaka University, Suita, Osaka, Japan

[6]National Research Center for Protozoan Diseases, Obihiro University of Agriculture and Veterinary Medicine, Obihiro, Hokkaido, Japan

***Corresponding author:** E-mail: kztanabe@biken.osaka-u.ac.jp.
Associate editor: Richard Thomas

Abstract

Mitochondrial (mt) genomes from diverse phylogenetic groups vary considerably in size, structure, and organization. The genus Plasmodium, causative agent of malaria, of the phylum Apicomplexa, has the smallest mt genome in the form of a circular and/or tandemly repeated linear element of 6 kb, encoding only three protein genes (*cox1*, *cox3*, and *cob*). The closely related genera Babesia and Theileria also have small mt genomes (6.6 kb) that are monomeric linear with an organization distinct from Plasmodium. To elucidate the structural divergence and evolution of mt genomes between Babesia/Theileria and Plasmodium, we determined five new sequences from *Babesia bigemina*, *B. caballi*, *B. gibsoni*, *Theileria orientalis*, and *T. equi*. Together with previously reported sequences of *B. bovis*, *T. annulata*, and *T. parva*, all eight Babesia and Theileria mt genomes are linear molecules with terminal inverted repeats (TIRs) on both ends containing three protein-coding genes (*cox1*, *cox3*, and *cob*) and six large subunit (LSU) ribosomal RNA (rRNA) gene fragments. The organization and transcriptional direction of protein-coding genes and the rRNA gene fragments were completely conserved in the four Babesia species. In contrast, notable variation occurred in the four Theileria species. Although the genome structures of *T. annulata* and *T. parva* were nearly identical to those of Babesia, an inversion in the 3-kb central region was found in *T. orientalis*. Moreover, the *T. equi* mt genome is the largest (8.2 kb) and most divergent with unusually long TIR sequences, in which *cox3* and two LSU rRNA gene fragments are located. The *T. equi* mt genome showed little synteny to the other species. These results suggest that the Theileria mt genome is highly diverse with lineage-specific evolution in two Theileria species: genome inversion in *T. orientalis* and gene-embedded long TIR in *T. equi*.

Key words: mitochondrion, mitochondrial genome, Babesia, Theileria, Plasmodium, Apicomplexa.

Introduction

Mitochondria, organelles essential for energy transduction and cellular functions, are present in almost all eukaryotes. Like nuclear genomes of eukaryotes, mitochondrial (mt) genomes from diverse phylogenetic groups vary considerably in size, structure, and organization as well as in the number of genes (Gray et al. 2004). The largest mt genome is found in land plants, in which the size ranges from 180 to 2,400 kb (Ward et al. 1981; Palmer et al. 1992), and the smallest is the 6-kb genome of the genus Plasmodium, causative agents of malaria. Plasmodium belongs to the phylum Apicomplexa, which includes >5,000 species, all of which are parasites of clinical or economic importance (Levine 1988). Veterinary and opportunistic pathogens include Babesia, which causes babesiosis in ruminants and humans; Theileria, causal agents for tropical theileriosis and East Coast fever in cattle; Cryptosporidium, responsible for cryptosporidiosis in humans and animals; and Toxoplasma, causing toxoplasmosis in immunocompromised patients and congenitally infected fetuses.

Relatively few apicomplexan mt genomes have been studied, and available data suggest that they are remarkably diverse in structure and genome organization. In Plasmodium, the mt genome is in the form of a circular and/or tandemly repeated, predominantly linear 6-kb element (Preiser et al. 1996; Wilson and Williamson 1997). The 6-kb element encodes only three mt protein-coding genes (cytochrome *c* oxidase subunits I and III: *cox1* and *cox3* and cytochrome *b*: *cob*) in addition to large subunit (LSU) and small subunit (SSU) ribosomal RNAs (rRNAs). The two rRNA genes are extensively fragmented and rearranged with 20 identified rRNA pieces, and curiously, no transfer RNA genes have

yet been identified (Feagin et al. 1997). The mt genomes of closely related apicomplexan parasites Babesia and Theileria (Lau 2009) are 6.6 kb in size and monomeric linear molecules with terminal inverted repeats (TIRs), indicative of telomeres (Kairo et al. 1994; Brayton et al. 2007). Similar to Plasmodium, mt genomes of Babesia and Theileria contain the three protein-coding genes, but gene order and transcriptional direction are clearly different from Plasmodium (Kairo et al. 1994; Brayton et al. 2007). Thus, the mt genomes of Plasmodium and Babesia/Theileria are structurally highly divergent regardless of their close relatedness (Kuo et al. 2008). For *Toxoplasma gondii*, the mt genome remains to be isolated and analyzed, although multiple copies of partial mt genes (*cox1* and *cob*) were found to be scattered throughout the nuclear genome (Ossorio et al. 1991). In *Cryptosporidium parvum*, the mitochondrion is degenerative and lacks any DNA (Abrahamsen et al. 2004). Clearly, the phylum Apicomplexa provides interesting materials to further understand the evolution of mt genomes.

It remains unknown how the remarkable structural divergence between Plasmodium and Babesia/Theileria mentioned above was generated. Gathering enough data set will also help provide further insights on the extent at which the mt genomes have evolved in the different genera as well as in the phylum. In this study, we determined five new mt genome sequences from Babesia and Theileria species. Analyses of the genome structures show that although the mt genome structure is conserved in Babesia species, it varies notably in both size and genome organization in Theileria species, with lineage-specific evolution in two Theileria species: genome inversion in *T. orientalis* and gene-embedded long TIR in *T. equi*.

Materials and Methods

Parasite Species

Mitochondrial genome sequences were determined from the following seven parasite species: *Babesia bigemina* (Kochinda stock) (Fujinaga et al. 1980), *B. caballi* (USDA strain) (Avarzed et al. 1997), *B. gibsoni* (National Research Center for Protozoan Diseases strain) (Ishimine et al. 1978), *B. bovis* (Miyama stock) (Fujinaga et al. 1980), *Theileria orientalis* (Ikeda stock) (Kim et al. 2004), *T. equi* (USDA strain) (Avarzed et al. 1998), and *T. parva* (Muguga stock) (Kairo et al. 1994). Their host animals are cattle for *B. bigemina*, *B. bovis*, *T. orientalis*, and *T. parva*; horses for *B. caballi* and *T. equi*; and dogs for *B. gibsoni* (supplementary table S1, Supplementary Material online).

DNA Sequencing

Parasite genomic DNA was extracted from animal bloods infected with *B. bigemina*, *B. gibsoni*, *B. bovis*, *T. orientalis*, and *T. parva*, and from cultures of *B. caballi* and *T. equi*, using QIAamp DNA Blood Mini Kit (QIAGEN, Hilden, Germany) according to the manufacturer's instructions. Nucleotide sequences of the mt genomes were determined by direct sequencing of polymerase chain reaction (PCR) products using specific primers (supplementary table S2a, Supplementary Material online). The primers were designed by aligning reported mt genome sequences of *B. bovis* (DDBL/EMBL/GenBank accession number EU075182), *T. parva* (Z23263), and *T. annulata* (NW_001091933). Amplification was carried out in a 20 μl reaction mixture containing 0.2 μM each of forward and reverse primers, 400 μM each of deoxynucleotide triphosphate (dNTP), 1 U of LA-Taq (Takara, Shiga, Japan), 2 μl of 10× PCR buffer, 2.5 mM of $MgCl_2$, and 1 μl of genomic DNA. PCR conditions were as follows: initial denaturation at 94 °C for 1 min and amplification for 40 cycles at 94 °C for 30 s, 55–68 °C (depending on primers used) for 30 s, and 72 °C for 1–6 min (depending on amplicon size, 1 min/kb), followed by a final extension at 72 °C for 10 min.

Sequences of the *T. equi* mt telomeric regions were determined by using the terminal deoxynucleotidyl transferase (TdT) tailing method (Bah et al. 2004) with some modifications. Briefly, the 3′ end was tailed with cytosine by initial denaturation of genomic DNA (150 ng) for 5 min at 95 °C and then incubated for 30 min at 37 °C in a reaction mixture containing 200 μM deoxycytidine triphosphate, 1 U of TdT (Takara), 20 mM Tris–HCl (pH 8.4), 50 mM KCl, and 1.5 mM $MgCl_2$, followed by heat inactivation of TdT at 65 °C for 10 min. The first PCR was done in a 50 μl reaction mixture containing 2 μl of the tailed DNA fragments, 1.25 U of AmpliTaq DNA Polymerase (Applied Biosystems, Foster City, CA), 2.5 mM $MgCl_2$, 200 μM dNTPs, 0.4 μM of an mt genome–specific primer (supplementary table S2b, Supplementary Material online), and a selective anchor primer (5′-CTACTACTACTAGGCCACGCGTCGACTAGTACGGGGGGGGGGGGGGG-3′). Initial denaturation was at 95 °C for 2 min, followed by 40 cycles at 94 °C for 30 s and 62 °C for 3 min, and with a final extension step at 72 °C for 10 min. The second PCR was performed using 1 μl of the first PCR product in a 50 μl reaction mixture mentioned above, containing a nested primer (supplementary table S2b, Supplementary Material online) and a universal amplification primer (5′-CTACTACTACTAGGCCACGCGTCGACTAGTAC-3′). The second PCR amplification was at 95 °C for 2 min, and 25 cycles of 94 °C for 30 s, 62 °C for 2 min, followed by an extension step at 72 °C for 10 min. This method would not work for the other Babesia and Theileria samples. It can be surmised that relatively high (A + T) content in TIRs of the other samples may have caused some problems. Multiple palindromes in TIR reported for *T. parva* (Shukla and Nene 1998) may also be contributing factors in the difficulty to determine telomeric sequences. In *T. equi*, unlike other Babesia and Theileria species, the TIR has a relatively low (A + T) content with no apparent multiple palindromes and, surprisingly, contains *cox3* and two fragments of rRNA gene (see Results).

TIR sequences of other Babesia and Theileria species were determined using an "inverted PCR," in which primers leading toward telomere ends (supplementary table S2b, Supplementary Material online) were used. We assumed that small inverted sequences, probably present in TIRs as reported for *T. parva* (Shukla and Nene 1998), could

self-anneal in opposite direction, enabling amplification of two telomeric regions encompassed by two outward primers when *Taq* polymerase with an exonuclease activity, that could excise unpaired bases (such as LA-Taq), was used. This inverted PCR successfully amplified specific DNA bands for all (Babesia and Theileria) but one species (i.e., *T. equi*) examined here.

PCR products were purified using QIAquick PCR Purification Kit (QIAGEN). DNA sequencing was performed directly from two independent PCR products using the BigDye Terminator v3.1 Cycle Sequencing Kit (Applied Biosystems) and an ABI 3130 Genetic Analyzer (Applied Biosystems). Sequencing primers were designed to cover target regions in both directions. DDBL/EMBL/GenBank accession numbers of sequences obtained in this study are given in supplementary table S1 (Supplementary Material online). The *T. parva* sequence obtained here has a 24-bp inconsistency with the reported *T. parva* sequence (Z23263). The *B. bovis* sequence in this study has a 7-bp difference from the reported *B. bovis* sequence (EU075182). These differences may be due to polymorphism because uncloned stock (*T. parva*) and different parasite strains (*B. bovis*) were used. We used our sequences of *T. parva* and *B. bovis* for analysis.

Gene Annotation

Nucleotide sequences of obtained mt genomes from Babesia and Theileria species and their deduced amino acid sequences were aligned together with reported sequences from *B. bovis* (EU075182), *T. parva* (Z23263), and *T. annulata* (NW_001091933) by ClustalW (Thompson et al. 1994). Alignment was manually corrected. Protein-coding genes were predicted using previously annotated sequences from *T. parva* and *B. bovis*.

To identify putative rRNA genes, mitochondrial DNA (mtDNA) sequences or annotated rRNA gene fragments from *B. bovis* (EU075182) and *T. parva* (Z23263) were used as queries under the suggested algorithm parameters (Freyhult et al. 2007) in NCBI BLAST 2.2 (Altschul et al. 1990). In silico analysis was also done with Probalign beta version 1.2 (Roshan et al. 2008) and SSEARCH 3.5 (Pearson 1991) using known rRNA gene fragments and suggested advanced search options (Freyhult et al. 2007; Roshan et al. 2008). Newly identified candidate rRNA genes were, likewise, used as input sequences. The information from sequence alignments using ClustalW (Thompson et al. 1994) and putative base-pairings between fragments proposed for *T. parva* mitochondrial ribosomal RNA fragments (Kairo et al. 1994) were considered in assigning the termini of the candidate genes. Similar searches using some of the rRNA fragment sequences from *Plasmodium falciparum* (Feagin et al. 1997) detected additional candidate gene regions.

Southern Blot Hybridization

Genomic DNA of *B. gibsoni*, *T. orientalis*, and *T. equi*, either undigested or digested with *Pvu*II, *Hind*III, or *Xho*I, was electrophoresed on 0.8% agarose gels in Tris–acetate–ethylenediaminetetraacetic acid (40 mM Tris–acetate and 1 mM ethylenediaminetetraacetic acid) and then transferred to a positively charged nylon membrane (Amersham Hybond-N+; GE Healthcare, Little Chalfont, England). PCR products amplified specifically from *B. gibsoni*, *T. orientalis*, and *T. equi* genomic DNA (supplementary table S2c, Supplementary Material online) were labeled with digoxigenin-deoxyuridine triphosphate using the DIG High Prime DNA Labeling and Detection Starter Kit II (Roche Diagnostics, Rotkreuz, Switzerland). The digoxigenin-labeled DNA probes were used for overnight hybridization. Blots were washed twice with 2× saline–sodium citrate (SSC) and 0.1% sodium dodecyl sulfate (SDS) and twice with 0.5× SSC and 0.1% SDS at 65 °C for 15 min. Hybridization signals were detected using the Detection Starter Kit II.

RNA Preparation and Analysis

Transcription of *cox1*, *cox3*, and *cob* in *B. gibsoni*, *T. orientalis*, and *T. equi* was analyzed by reverse transcriptase-PCR (RT-PCR). Total RNA was extracted with RNeasy Mini Kit (QIAGEN). DNase I treatment was done to remove any residual DNA before cDNA synthesis. Using specific primers (supplementary table S2d, Supplementary Material online), cDNA synthesis and DNA amplification were carried out using PrimeScript High Fidelity RT-PCR Kit (Takara). RNA extracts that were not treated with reverse transcriptase gave no PCR products.

For northern blot analysis, total RNA including short RNAs from *B. gibsoni* was prepared with mirVana miRNA Isolation Kit (Ambion, Austin, TX). Total RNA (10 μg) was subjected to 8.3 M urea-12% (w/v) polyacrylamide gel electrophoresis. After electrophoresis, the gel was stained with ethidium bromide and photographed. RNA was electroblotted on Biodyne Plus (Pall, Glen Cove, NY) using a semi-dry blotter NA-1515B (Nihon Eido, Tokyo, Japan) according to the manufacturer's protocol. The blotted membrane was ultraviolet treated for cross-linking (Brown et al. 2004) and incubated in hybridization solution (200 mM sodium phosphate [pH 7.2]-7% [w/v] SDS) for 30 min at 37 °C. The oligo probe was 5′ labeled with T4 polynucleotide kinase and [γ-^{32}P] adenosine triphosphate according to the enzyme supplier's instruction (Takara) and purified based on Brown et al. (2004). After overnight hybridization at 37 °C, the membrane was then washed twice with 2× SSC-0.5% (w/v) SDS at 37 °C, twice at 47 °C, and finally twice with 0.2× SSC-0.5% (w/v) SDS at 47 °C. The membrane was exposed to an Imaging Plate (Fujifilm, Tokyo, Japan), and the plate was scanned with a BAS2500 Bioimaging Analyzer (Fujifilm).

Phylogenetic Analysis

The concatenated amino acid sequences of *cox1* and *cob* were used for phylogenetic analysis. (Sequences of *cox3* were not used due to very high divergence in Babesia/ Theileria species [see Results].) The data set of 834 amino acid positions, comprising 474 COX1 and 360 COB amino acids, was analyzed using the PROML program in PHYLIP version

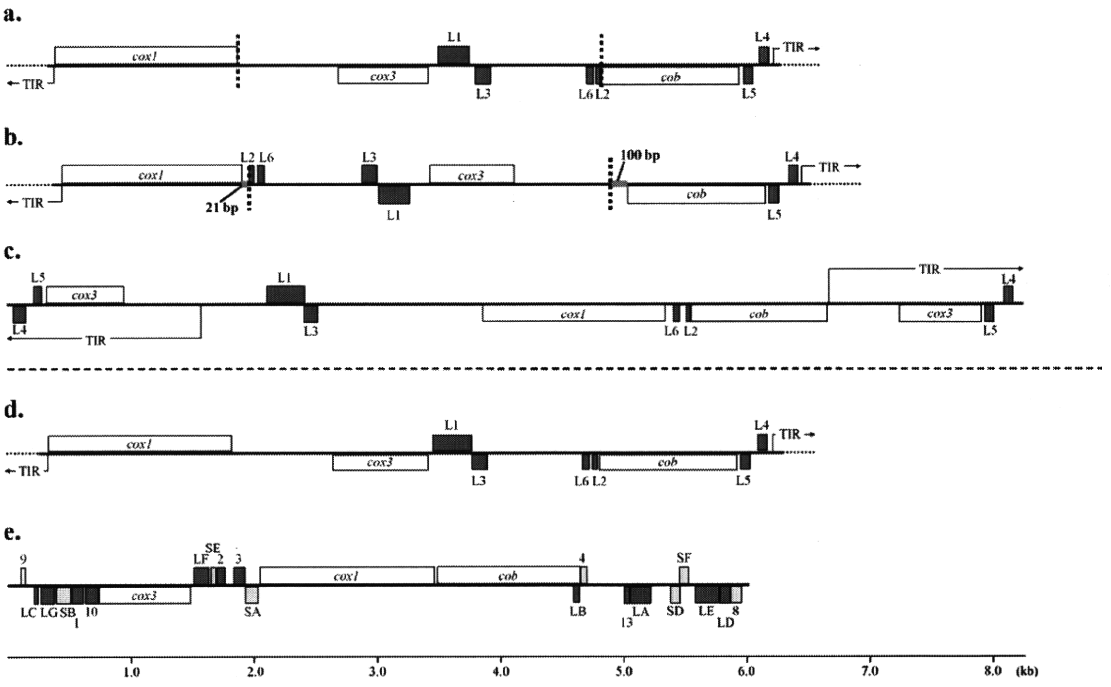

FIG. 1. Structure of the mitochondrial genomes of *Babesia gibsoni* (*a*), *Theileria orientalis* (*b*), and *T. equi* (*c*). Mitochondrial (mt) genome structure was completely conserved among *B. gibsoni*, *B. bigemina* (not shown), *B. caballi* (not shown), *B. bovis* (not shown), and *T. parva* (*d*). The *T. orientalis* mt genome has an inversion in the 3-kb central region. The *T. equi* mt genome has a relatively long TIR and contains a *cox3* gene and rRNA gene fragments. Shown for comparison is the mt genome of *Plasmodium falciparum* (*e*) (Feagin et al. 1997). Genes shown above the bold line in each genome are transcribed left to right and those below are transcribed from right to left. Two small gray lines in the *T. orientalis* genome indicate an inversion. Vertical broken lines indicate the boundaries of the 3-kb inversion. Dark and light gray boxes indicate fragments of LSU and SSU rRNA genes, respectively. *cox1*, cytochrome *c* oxidase subunit I; *cox3*, cytochrome *c* oxidase subunit III; *cob*, cytochrome *b*.

3.68 (Felsenstein and Churchill 1996) under the Jones, Taylor, and Thornton model (Jones et al. 1992) with the amino acid frequencies of the data set used to infer the maximum likelihood (ML) tree. Corresponding sequence of *P. falciparum* was used as an outgroup. To take the evolutionary rate heterogeneity, the R option was set to utilize discrete Γ distribution with eight categories for approximating the site rate distribution. CODEML program in PAML version 4.2 (Yang 2007) was used to estimate the Γ shape parameter value α. Bootstrap analysis was done by applying PROML to 100 resampled data sets produced by SEQBOOT program in PHYLIP. Bootstrap proportion (BP) values were calculated for internal branches of the inferred ML tree using CONSENSE in PHYLIP.

LSU sequences (592 sites in total: 265 bp for LSU1; 35 bp for LSU2; 111 bp for LSU3; 82 bp for LSU4; 64 bp for LSU5; and 35 bp for LSU6) were analyzed using the ML method performed with PAUP* 4.0 b10 (Swofford 2002). The appropriate nucleotide substitution model was first determined using the Modeltest (version 3.7) estimations, including both the proportion of invariable sites and the Γ shape parameter (Posada and Crandall 1998). For branch support of the ML tree, bootstrap probability was estimated from 1,000 heuristic replicates with single random addition replicates. All trees were reconstructed with TreeView 1.6.6 (Page 1996). For statistical comparisons among the ML best tree and its alternatives, *P* values of Kishino–Hasegawa (KH) test (Kishino and Hasegawa 1989) and Simodaira–Hasegawa (SH) test (Shimodaira and Hasegawa 1999) were obtained.

Results

Mitochondrial Genome Organization

We obtained 5.8- to 5.9-kb sequences from each of *B. bigemina*, *B. caballi*, *B. gibsoni*, and *B. bovis*, in which three protein-coding genes, *cox1*, *cox3*, and *cob*, and five fragments of the LSU rRNA gene were identified (fig. 1*a*). TIR sequences were also found on both ends of the predicted linear mt genomes. Although full-length sequences of TIRs were not successfully determined, the size of the TIR was inferred to be 440–450 bp from results of Southern blot hybridization analysis (see below). Additionally, we identified one LSU fragment of rRNA gene, LSU6, that showed a high sequence similarity to the 3′ part of RNA10 of the *P. falciparum* rRNA gene fragment (Feagin et al. 1997) (underlined sequence in the following *B. gibsoni* LSU sequence are identical nucleotides to *P. falciparum*

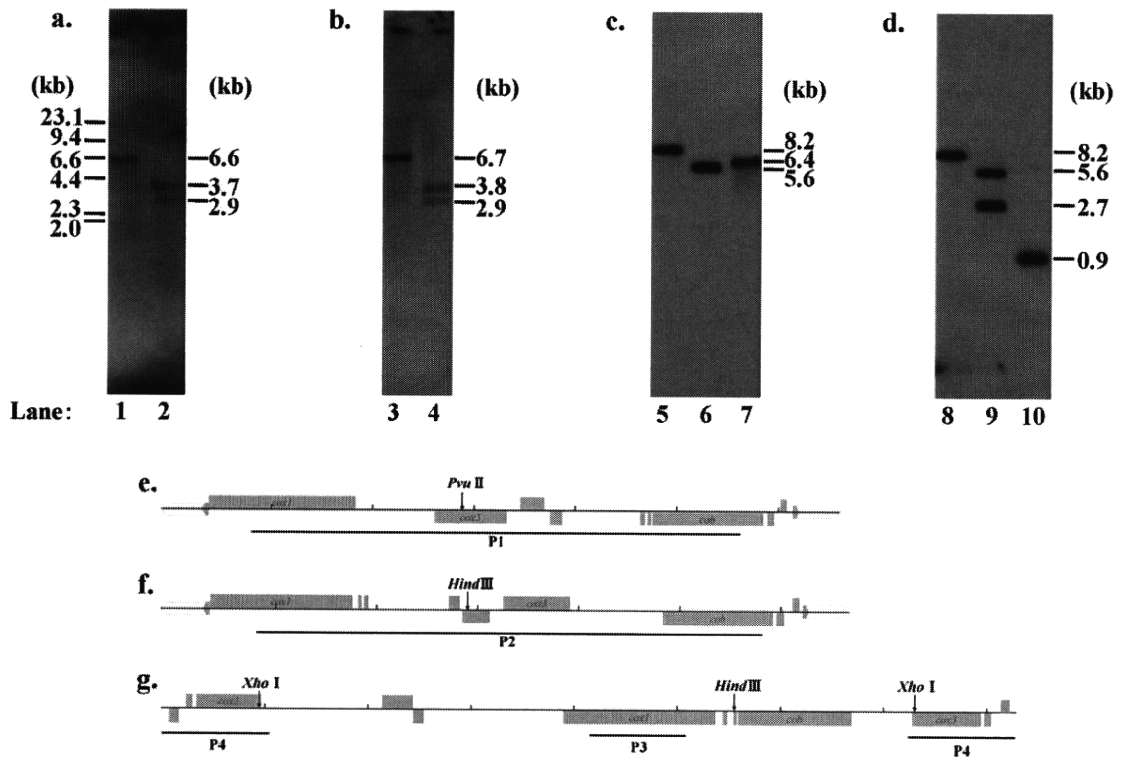

FIG. 2. Monomeric linear structure of the mitochondrial genomes of *Babesia gibsoni*, *Theileria orientalis*, and *T. equi*. Genomic DNA of *B. gibsoni* (*a*), *T. orientalis* (*b*), and *T. equi* (*c* and *d*) was hybridized with a *B. gibsoni* probe P1 (*e*), a *T. orientalis* probe P2 (*f*), and *T. equi* probes P3 and P4 (*g*), respectively. Undigested DNA (lanes 1, 3, 5, and 8) or DNA digested with *Pvu*II (lane 2), *Hind*III (lanes 4, 6, and 9), or *Xho*I (lanes 7 and 10) was fractionated on 0.8% agarose gels.

RNA10: 5′-ATAGCCGGAGTACGTAAGGAATAGGAAA-GATTAACCGCTATCA-3′). The organization and predicted transcriptional direction of the three protein-coding genes and the six LSU rRNA gene fragments were completely conserved among *B. bigemina*, *B. caballi*, *B. gibsoni*, *B. bovis*, *T. parva*, and *T. annulata* (fig. 1*a*). Southern blots probed with a 4.9-kb portion (P1) of the *B. gibsoni* mt genome produced a clear signal at 6.6 kb against *B. gibsoni* genomic DNA and two bands at 3.7 and 2.9 kb against DNA digested with *Pvu*II (fig. 2*a* and *e*). The sizes of the two bands were identical to those predicted from the sequence. These results confirm the monomeric linear 6.6 kb of *B. gibsoni* mt genome similar to that reported for *T. parva* and *T. annulata* (Hall et al. 1990; Kairo et al. 1994).

Interestingly, the *T. orientalis* mt genome, aside from having three protein-coding genes, six rRNA gene fragments, and TIRs similar to four Babesia species, *T. parva*, and *T. annulata* (fig. 1*b*) showed an inversion at the 3.0-kb central region containing *cox3*, LSU1, LSU3, LSU6, and LSU2. No sequences that potentially form secondary structures such as a hairpin structure were apparent near the boundaries of this inverted sequence, but instead, unique insertions of 21–22 and 84–102 bp were noted (fig. 1*b*), making the *T. orientalis* mt genome slightly longer (112–168 bp) than the other six Babesia and Theileria mt genomes (supplementary table S3, Supplementary Material online). As predicted from the sequence, southern hybridization using a *T. orientalis* probe (P2) that spans the central 5.0-kb region yielded a band at 6.7 kb against undigested DNA and two bands at 3.8 and 2.9 kb against *Hind*III-digested DNA (fig. 2*b* and *f*). From these results, the *T. orientalis* mt genome shows a 6.7-kb monomeric linear structure.

Strikingly distinctive from all other mt genomes described above is *T. equi*. First, the size of the *T. equi* genome is 8.2 kb, that is, 1.6–1.7 kb longer than that of other species. Second, TIR sequences are large (1,563 bp), compared with the 440–450 bp TIRs of the other seven species, and, interestingly, contained *cox3* and two LSU rRNA gene fragments, LSU4 and LSU5. TIR sequences on both ends showed complete identity. Third, the protein-coding genes and rRNA gene fragments showed little synteny to other species (fig. 1*c*). Hybridization with a probe corresponding to a 1.0-kb region in *cox1* (P3) produced a band at 8.2 kb against undigested DNA, a band at 5.6 kb against *Hind*III-digested DNA, and a band at 6.4 kb against *Xho*I-digested DNA (fig. 2*c* and *g*). Another *T. equi* probe using a 1-kb region in the TIR (P4) produced a band at 8.2 kb against undigested DNA, two bands at 5.6 and 2.7 kb against *Hind*III-digested DNA, and a band at 0.9 kb against

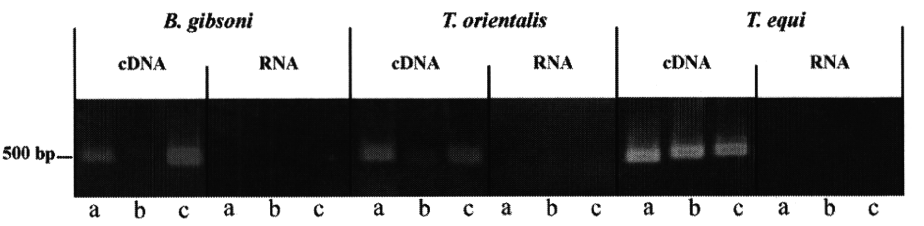

FIG. 3. Transcription of the three protein-coding genes *cox1* (*a*), *cox3* (*b*), and *cob* (*c*) in the mitochondrial genome of *Babesia gibsoni*, *Theileria orientalis*, and *T. equi*. See Materials and Methods for details.

*Xho*I-digested DNA (fig. 2*d* and *g*). The sizes of these bands match the predicted *T. equi* sequence, indicating an 8.2-kb monomeric linear structure of the *T. equi* mt genome.

Transcription

RT-PCR using three separate primer sets targeting about 500-bp sequences of *cox1*, *cox3*, and *cob* of *B. gibsoni* gave the expected transcript size using cDNA but not using RNA (fig. 3). Similarly, expected PCR sized fragments were obtained using primers specific to *T. orientalis* or *T. equi* for *cox1*, *cox3*, and *cob*. Results confirm the transcription of the three protein-coding genes, including *cox3* in the 3-kb inverted region of *T. orientalis* and *cox3* in TIR of *T. equi*.

Transcription of LSU6 was confirmed by northern blot analysis. Probing with two oligonucleotides (18-mer and 23-mer at the 5′ and 3′ end, respectively) complementary to LSU6 against *B. gibsoni* total RNA produced approximately 90-nt RNA signal (fig. 4), suggesting that the LSU6 was actually transcribed and the corresponding stable transcript existed as a short RNA fragment. Due to extreme difficulties in obtaining an adequate amount of parasites from infected hosts and/or in vitro culture limitations for *B. bigemina*, *B. caballi*, *T. orientalis*, and *T. equi*, we were unable to perform additional northern blot analyses. Together with the report of Kairo et al. (1994) on the transcription of the three protein-coding genes and five known LSU rRNA gene fragments (LSU1–LSU5) in *T. parva*, however, these results suggest that both protein genes and rRNA gene fragments are transcribed in Babesia and Theileria.

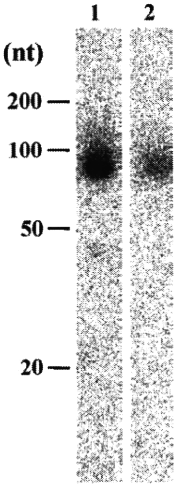

FIG. 4. Transcription of the *Babesia gibsoni* mt genome LSU6. *B. gibsoni* total RNA was probed with oligonucleotides complementary to the putative LSU6 fragment. Probe sequences: lane 1, TGATAGCGGTTAATCTTTCCTAT; lane 2, CTTACGTACTCCGGCTAT. Positions and sizes (in nucleotides [nt]) of marker RNAs (DynaMarker RNA Low II; BioDynamics Laboratory) are shown.

Sequence Similarity and Phylogeny

cox1 and *cob* pairwise sequence similarity scores among *B. bovis*, *B. bigemina*, *B. caballi*, *B. gibsoni*, *T. parva*, *T. orientalis*, *T. annulata*, and *T. equi* were comparable: 67–88% for *cox1* and 60–85% for *cob* at the amino acid sequence level (supplementary table S4, Supplementary Material online). Conserved sequence regions in COX1 and COB correspond to the 12 and 9 transmembrane domains as inferred from bovine COX1 (SWISS-PROT protein database accession number P00396) and COB (P00157), respectively, in which multiple heme-binding histidine residues that form catalytic sites are perfectly conserved (Widger et al. 1984; Yun et al. 1991; Castresana et al. 1994; Ferguson-Miller and Babcock 1996). For *cox3*, pairwise sequence similarity was relatively low, and *T. equi* *cox3* in particular has considerably low similarity to *cox3* of other species (37–41% compared with the 57–80% similarity of other *cox3* in Babesia and Theileria species). Nevertheless, the predicted *T. equi* COX3 amino acid sequence shows seven transmembrane domains (from I to VII) and the C-terminal hydrophobic domain VII (P00415) that are highly conserved among a wide variety of organisms from prokaryotes to plants (Haltia et al. 1991). In contrast to these protein-coding genes, pairwise sequence similarity of six LSUs was very high, 75–96% among all the Babesia and Theileria species examined here (supplementary table S5, Supplementary Material online).

The ML tree was inferred from concatenated COX1 and COB amino acid sequences using *P. falciparum* as an outgroup (fig. 5). Monophyletic relationships were observed with high BP values (98%) for 1) *B. bovis*, *B. bigemina*, *B. caballi*, and *B. gibsoni* and 2) *T. annulata*, *T. parva*, and *T. orientalis*. *Theileria equi* was located at the branch

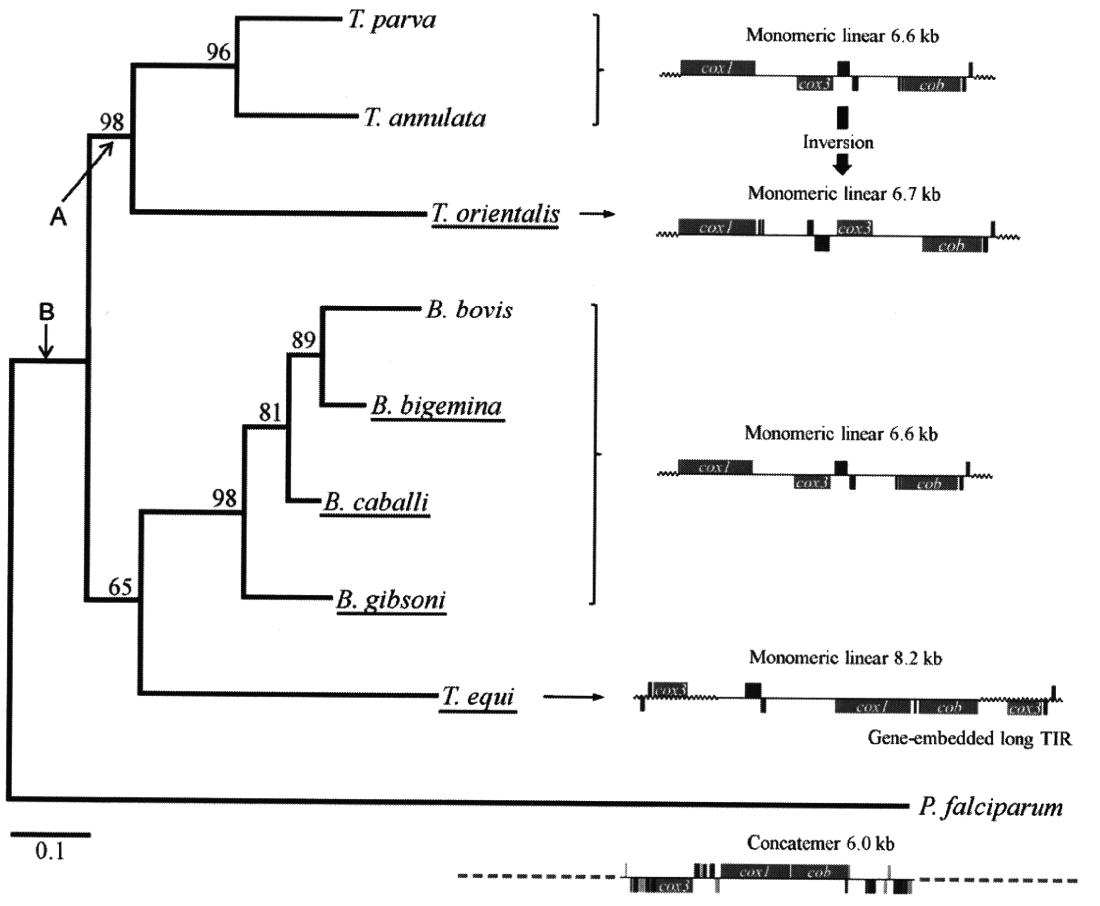

FIG. 5. The ML phylogenetic tree of the two mitochondrial protein-coding genes, *cox1* and *cob*, from eight Babesia and Theileria species. *Plasmodium falciparum* was used as an outgroup. Concatenated amino acid sequences (834 sites) were used with 1,000 heuristic replicates under a Jones, Taylor, and Thornton model ($\alpha = 0.72$). The numbers shown along nodes represent bootstrap values. Arrows, A and B, indicate alternative positions of the *Theileria equi* sequence, whose possibilities were statistically compared by the SH and KH tests. Five parasite sequences obtained in this study are underlined.

leading to the common ancestor of Babesia species with moderate BP value (65%). The other possible branching positions of *T. equi* at the ancestral branch of Theileria (arrow A in fig. 5) or at the ancestral branch of Theileria and Babesia (arrow B in fig. 5) were, however, not rejected by either the KH or the SH tests (supplementary table S6, Supplementary Material online), thus indicating that the evolutionary position of *T. equi* is yet unclear with the present data set.

The ML tree constructed using LSU sequences was basically the same as that of *cox1* and *cob* (supplementary fig. S1, Supplementary Material online), although, in this case, unrooted trees were compared because an appropriate outgroup species is not available for LSU. Monophyletic relationships of the four Babesia species and of *T. annulata*, *T. parva*, and *T. orientalis* were supported with high BP values. Within the clade of Babesia, however, the relationship between *B. bovis*, *B. bigemina*, and *B. caballi* was not supported with high BP values and not highly consistent to that in the *cox1*/*cob* tree. Notably, when the data set of LSU was applied to the two topologies, one for the *cox1*/*cob* tree and the other for the LSU tree, the two trees were not significantly different (data not shown), suggesting that the relationship of the three Babesia species was not clearly separable using the LSU sequences.

Partial TIR sequences (47–1,563 bp) (supplementary table S3, Supplementary Material online) were highly divergent among all eight Babesia and Theileria species examined here. In noncoding regions excluding TIR, we identified 14 sequence regions that were highly similar among all the Babesia and Theileria species (fig. 6 and supplementary tables S7 and S8, Supplementary Material online). Pairwise sequence similarity of these 14 regions ranged from 81% to 97%, values comparable with LSUs. The array and direction of the 14 regions were well conserved among (including the inverted region of *T. orientalis*), but one, species. *Theileria equi* was the exception, in which case the 14 regions were extensively

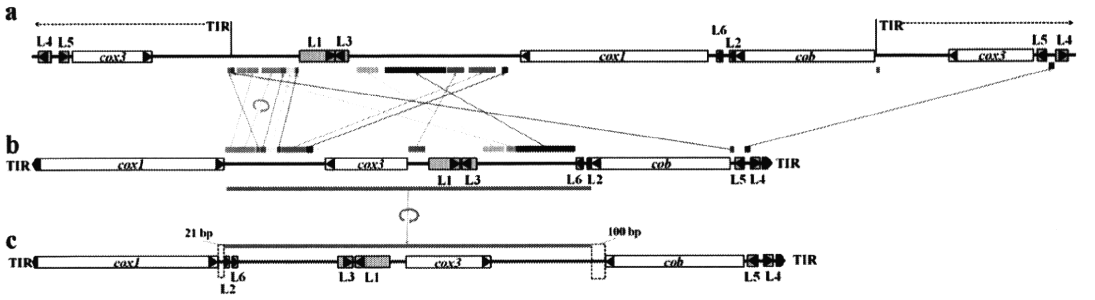

FIG. 6. Arrangement of small noncoding sequence regions in the mitochondrial genome highly conserved between *Theileria equi* (*a*), *Babesia gibsoni* (*b*), and *T. orientalis* (*c*). Those sequences are indicated by matched colored bars and arrows. A 3.0-kb inversion in the *T. orientalis* mt genome is shown by green bars with a circular arrow in (*b*) and (*c*). *cox1*, cytochrome *c* oxidase subunit I; *cox3*, cytochrome *c* oxidase subunit III; *cob*, cytochrome *b*.

rearranged (fig. 6). Within species, these 14 regions did not show sequence similarity to each other.

Discussion

This study presents for the first time evidence of the highly divergent mt genomes in the genus Theileria and a high conservation in the genus Babesia. *Theileria annulata* and *T. parva* have an mt genome structure nearly identical to that of Babesia, whereas the mt genomes of *T. orientalis* and *T. equi* were clearly distinctive: a large genomic region is inverted in *T. orientalis*, and in *T. equi*, there occurs an unusually long TIR, containing *cox3* and two LSU rRNA gene fragments. The phylogenetic tree of *cox1*/*cob* showed two separate clades: one for three Theileria species (*T. parva*, *T. annulata*, and *T. orientalis*) and another for four Babesia species. The mt genome structures of these Theileria species are highly conserved. This suggests that an inversion event occurred specifically in the *T. orientalis* lineage after divergence from a common ancestor of *T. annulata*, *T. parva*, and *T. orientalis*. The phylogenetic position of *T. equi* was not clearly determined in the *cox1*/*cob* tree. This unclear positioning of *T. equi* is consistent with the tree based on 18S rRNA gene, a nuclear genome gene (Criado-Fornelio et al. 2003). Thus, it remains to be solved whether a common ancestor of *T. equi*, the Theileria clades, and Babesia clades possessed an mt genome with gene-embedded long TIR. Phylogenetic separation of *T. equi* from Theileria clade as well as the identical life cycle, namely, the presence of schizogony in lymphocytes and lack of transovarial transmission by vector (Uilenberg 2006), suggests that, most likely, the mt genome of the common ancestor contained a long TIR.

Compared with moderate sequence similarity in *cox1* and *cob* of Theileria and Babesia species, *cox3* is highly divergent. Similarly, *cox3* is more divergent than *cox1* and *cob* in Plasmodium species (Wilson and Williamson 1997; Perkins 2008). COB is a subunit of complex III, essential for electron transfer in the mitochondrial respiratory chain (Xia et al. 1997). COX1 (subunit I) (and also COX2 [subunit II]), which contains heme and copper and is essential for electron transfer, is 1 of 13 subunits of cytochrome *c* oxidase (complex IV), a terminal oxidase in the respiratory chain (Castresana et al. 1994). COX3, which is not directly involved in the electron transport, is considered to stabilize the complex of COX1 and COX2 (Haltia et al. 1991; Tsukihara et al. 1996). Such an accessory role of COX3 in the function of cytochrome *c* oxidase may relax constraints, causing acceleration of evolutionary rate and low sequence similarity.

In addition to the five previously known LSU rRNA gene fragments (LSU1–LSU5) (Kairo et al. 1994; Brayton et al. 2007), we newly identified an LSU fragment, LSU6, in all Babesia and Theileria species, whose transcription was confirmed by northern blot analysis. Kairo et al. (1994) have previously mapped LSU1–LSU5 (by comparative secondary structure modeling) to the 3′ half of *Escherichia coli* 23S (LSU) rRNA. LSU5 and 5′ region of LSU1 form the domain IV of LSU, whereas 3′ region of LSU1, LSU2, LSU3, and LSU4 forms the domain V of the LSU, which contains the peptidyl transferase center. We mapped the newly identified LSU6 to positions 2640–2670, which forms a part of the domain VI (alpha-sarcin/ricin stem loop) of the LSU. Contrary to the other LSU fragments, the borders of LSU6 were unclear because the flanking sequences have no recognizable complementarities to other fragments. In addition to LSU6, we found a small sequence region in all Babesia and Theileria mtDNA, which showed a high sequence similarity to a small subunit fragment (SSUF) of the *P. falciparum* rRNA gene. We were not, however, able to confirm transcription of the SSUF (data not shown), although the region is regarded as one of the highly similar noncoding regions (supplementary table S7, Supplementary Material online). The mtDNA of Babesia/Theileria still contains large unannotated sequence regions (about one-third sequence regions of the genome), and those sequences are highly conserved among parasite species of the two genera (supplementary table S8, Supplementary Material online). It is thus likely that unidentified rRNA gene fragments as well as other genes exist in these regions. Comprehensive and detailed mtDNA transcript analysis of Babesia/Theileria would be required for further identification of genes and gene fragments as was done for *P. falciparum* (Feagin et al. 1997).